1 **circZNF827 nucleates a transcription inhibitory complex to balance**

2 **neuronal differentiation**

3

4 Anne Kruse Hollensen[1], Henriette Sylvain Thomsen[1], Marta Lloret-Llinares[1,2],

5 Andreas Bjerregaard Kamstrup[1], Jacob Malthe Jensen[3], Majbritt Luckmann[1],

6 Nanna Birkmose[1], Johan Palmfeldt[4], Torben Heick Jensen[1], Thomas Birkballe

7 Hansen[1] and Christian Kroun Damgaard[1§]

8

9 [1]Department of Molecular Biology and Genetics, Aarhus University, C.F.

10 Møllers Allé 3, Building 1130, DK-8000 Aarhus C, Denmark

11 [2]European Bioinformatics Institute (EMBL-EBI), European Molecular Biology

12 Laboratory, Wellcome Genome Campus, Hinxton, Cambridge CB10 1SD UK.

13 [3]Bioinformatics Research Centre, Aarhus University, C.F. Møllers Allé 8,

14 Building 1110, DK-8000 Aarhus C, Denmark Denmark

15 [4]Department of Clinical Medicine, Research Unit for Molecular Medicine,

16 Aarhus University, Palle Juul-Jensens Boulevard 99, DK-8200 Aarhus N,

17 Denmark

18

19

20 [§]Corresponding author

21

22

Abstract

Circular RNAs are important for many cellular processes but their mechanisms of action remain poorly understood. Here, we map circRNA inventories of mouse embryonic stem cells, neuronal progenitor cells and differentiated neurons and identify hundreds of highly expressed circRNAs. By screening several candidate circRNAs for a potential function in neuronal differentiation, we find that circZNF827 represses expression of key neuronal markers, suggesting that this molecule negatively regulates neuronal differentiation. Among 760 tested genes linked to known neuronal pathways, knockdown of circZNF827 deregulates expression of numerous genes including nerve growth factor receptor (NGFR), which becomes transcriptionally upregulated to enhance NGF signalling. We identify a circZNF827-nucleated transcription-repressive complex containing hnRNP-K/L proteins and show that knockdown of these factors strongly augments NGFR regulation. Finally, we show that ZNF827 protein is part of the mRNP complex, suggesting a functional co-evolution of a circRNA and the protein encoded by its linear pre-mRNA host.

1 Introduction

2

3 The mammalian non-coding transcriptome, which includes long noncoding

4 RNAs (lncRNAs) and circular RNAs (circRNAs), plays pivotal roles in biological

5 decisions during differentiation and normal cell maintenance (reviewed in

6 (Chekulaeva & Rajewsky, 2018; Deveson, Hardwick, Mercer, & Mattick, 2017;

7 Kopp & Mendell, 2018)). Even though circRNAs were already identified several

8 decades ago (Capel et al., 1993; Kos, Dijkema, Arnberg, van der Meide, &

9 Schellekens, 1986; Nigro et al., 1991; Sanger, Klotz, Riesner, Gross, &

10 Kleinschmidt, 1976), they only recently have emerged as a large class of

11 abundant noncoding RNAs that exhibit cell type- and tissue-specific expression

12 patterns (Ashwal-Fluss et al., 2014; Hansen et al., 2013; Jeck et al., 2013;

13 Memczak et al., 2013; Rybak-Wolf et al., 2015; Salzman, Chen, Olsen, Wang,

14 & Brown, 2013; Salzman, Gawad, Wang, Lacayo, & Brown, 2012) (reviewed in

15 (Chekulaeva & Rajewsky, 2018; Ebbesen, Hansen, & Kjems, 2016; Salzman,

16 2016)). CircRNAs are generated by the canonical spliceosome in a non-linear

17 backsplicing fashion (Cocquerelle, Mascrez, Hetuin, & Bailleul, 1993; Jeck et

18 al., 2013; Memczak et al., 2013; Pasman, Been, & Garcia-Blanco, 1996;

19 Salzman et al., 2012). During circRNA biogenesis, flanking intronic sequences

20 are thought to bring splice sites within critically close proximity, either by direct

21 basepairing between inverted repeats (e.g. Alu-repeats) or facilitated by

22 interactions between flanking intron-bound RNA-binding proteins (RBPs)

23 (Ashwal-Fluss et al., 2014; Conn et al., 2015; Ebbesen et al., 2016). Most

24 circRNAs are primarily localized to the cell cytoplasm (Ashwal-Fluss et al.,

25 2014; Hansen et al., 2013; Jeck et al., 2013; Memczak et al., 2013; Rybak-Wolf

1   et al., 2015; Salzman et al., 2012), and recent evidence suggests that nuclear

2   export of circRNAs in human cells is influenced by the size of the given

3   molecules, where larger circRNAs (>800 nucleotides) are dependent on

4   DExH/D-box helicase UAP56 (DDX39B), whereas smaller species are

5   dependent on URH49 (DDX39A)(Huang, Liang, Tatomer, & Wilusz, 2018).

6

7   Several reports have provided evidence that circRNAs play important roles in

8   various fundamental cellular processes. Well described examples are the

9   CDR1as/ciRS-7 and SRY circRNAs that function to negatively regulate miR-7

10   and miR-138 activity, respectively, by sequestration (miRNA sponging), leading

11   to increased mRNA expression of their respective miRNA-targets (Hansen et

12   al., 2013; Memczak et al., 2013). However, it has also been suggested that the

13   majority of circRNAs are likely not *bona fide* miRNA sponges, simply due to

14   relatively low copy numbers and a low number of miRNA binding sites per

15   molecule, leaving efficient miRNA regulation ambigous in many cases

16   (Chekulaeva & Rajewsky, 2018; Ebbesen et al., 2016). Examples of circRNAs

17   acting as binding scaffolds for RBPs, or RBP sponges, which in turn affect their

18   canonical function in e.g. pre-mRNA splicing and protein translation, have been

19   reported (Abdelmohsen et al., 2017; Ashwal-Fluss et al., 2014). Nuclear

20   variants coined exon-intron circular RNAs (ElciRNAs), have, due to their

21   retention of intronic sequences, been shown to promote transcription by

22   recruitment of U1 snRNP to transcription units by a not fully clarified mechanism

23   (Li et al., 2015). Many abundant circRNAs originate from the 5' end of their

24   precursor transcripts, often giving rise to backsplicing into parts of the 5'UTR of

25   their linear relative (Jeck et al., 2013; Memczak et al., 2013; Rybak-Wolf et al.,

4

1   2015). The prevalence af these AUG circRNAs suggests that at least a subset

2   of circRNAs could have protein-coding potential via a cap-independent

3   translation mechanism (Stagsted, Nielsen, Daugaard, & Hansen, 2019). This is

4   consistent with both early studies of Internal Ribosome Entry Sites (IRES)

5   placed in a circRNA context (Chen & Sarnow, 1995), as well as more recent

6   studies reporting examples of translation-competent circRNAs (AbouHaidar,

7   Venkataraman, Golshani, Liu, & Ahmad, 2014; Legnini et al., 2017; Pamudurti

8   et al., 2017; Yang et al., 2017). However, global analyses of hundreds of

9   ribosome profiling and mass-spec datasets, suggests that these few examples

10 are specialized events, and not a generally applicable function of circRNAs

11 (Stagsted et al., 2019).

12

13 RNA-sequencing of RNA isolated from mouse and human tissues along with

14 various cell lines suggests that circRNAs are most abundantly expressed in the

15 brain, compared to other tissues and that circRNAs are particular enriched in

16 neuronal synaptosomes (Rybak-Wolf et al., 2015). In line with this, cells derived

17 from both embryonal carcinoma (P19) and neuroblastoma (SHSY-5Y)

18 subjected to neuronal/glial differentiation show tightly regulated circRNA

19 expression profiles during neuronal development, that include upregulation of

20 numerous common circRNAs (Rybak-Wolf et al., 2015). Piwecka et al.,

21 demonstrated that a ciRS-7 knockout mouse displayed downregulated miR-7

22 levels, alterations in sensorimotor gating associated with neuropsychiatric

23 disease and abnormal synaptic transmission, suggesting that ciRS-7 and miR-

24 7 are important for normal brain function in the mouse (Piwecka et al., 2017).

25 Adding to the complexity of this regulatory network, a long noncoding RNA

5

1   (lncRNA), Cyrano, promotes the destruction of miR-7, which in turn upregulates

2   ciRS-7 by a still unidentified mechanism (Kleaveland, Shi, Stefano, & Bartel,

3   2018). One circRNA, circSLC45A4, which is very abundant in the cortex of the

4   mouse and human brain, has recently been shown to negatively regulate

5   neuronal differentiation, both in cell cultures and in developing mice, where its

6   knockdown dysregulates the balance between specialized cortex neurons by

7   unknown molecular mechanisms (Suenkel, Cavalli, Massalini, Calegari, &

8   Rajewsky, 2020).

9

10 Despite these intricate molecular interactions between circRNA, miRNA and

11 lncRNA, many important questions regarding neuronal differentiation and

12 function remain unanswered. For example, it is largely unknown how the tightly

13 controlled expression of circRNAs potentially affects neuronal development.

14 Here, we present the circRNA inventory of mouse embryonic stem cells

15 (mESC), neuronal progenitor cells (NPC) and differentiated glutamatergic

16 neurons, which represents a well-established model for CNS-type neuronal

17 differentiation (Bibel, Richter, Lacroix, & Barde, 2007). We report thousands of

18 RNase R-resistant circRNAs of which many are differentially regulated during

19 neuronal development. In a screen for circRNA function using an established

20 human model for neuronal differentiation, we identify circZNF827 as a negative

21 regulator of neuronal differentiation. Although being almost exclusively

22 localized to the cell cytoplasm, the nuclear population of this circRNA impacts

23 several genes of relevance in neuronal differentiation, at the level of

24 transcription, including nerve growth factor receptor (NGFR), which becomes

25 robustly upregulated upon circZNF827 knockdown. Mechanistically, our

6

1 evidence suggests that circZNF827 is a necessary scaffold for a transcription-

2 repressive complex containing its own host-encoded protein; ZNF827, together

3 with hnRNP K and hnRNP L.

4

5

1 evidence suggests that circZNF827 is a necessary scaffold for a transcription-

7

2 repressive complex containing its own host-encoded protein; ZNF827, together

3 with hnRNP K and hnRNP L.

1   **Results**

2

3   *The circRNA profile of mESCs changes markedly upon neuronal differentiation*

4   To determine whether circRNAs can influence neuronal differentiation, we

5   initially mapped the circRNA inventories at different stages of neuronal

6   differentiation and compared these to other available circRNA datasets of

7   neuronal origin from mice and humans (Rybak-Wolf et al., 2015). Identification

8   of circRNAs from RNA-seq experiments has often been based on quantification

9   of relatively few reads across the circRNA backsplicing junction (circBase

10   (Glazar, Papavasileiou, & Rajewsky, 2014)), and current circRNA prediction

11   algorithms inevitably lead to the calling of false positives(Hansen, Veno,

12   Damgaard, & Kjems, 2016; Jeck & Sharpless, 2014). Hence, to immediately

13   validate the circular nature of *to-be* called circRNAs, we first performed

14   standard rRNA depletion and subsequently either included or excluded RNase

15   R treatment step prior to RNA-sequencing. Specifically, we used an established

16   differentiation model for CNS-type glutamatergic neurons, based on E14

17   mouse embryonic stem cells (mESCs) that reportedly yields a purity of

18   glutamatergic neurons of >90% (Bibel et al., 2007). RNA was isolated from 3

19   stages of differentiation, mESCs, neuronal progenitor cells (mNPCs) or

20   neuronal differentiation day 8 (mN8) and rRNA depleted (+/- RNase R) prior to

21   library preparation and RNA-seq (Figure 1A). Successful differentiation at the

22   NPC and N8 stages was confirmed by the appearance of elongated inter-

23   cellular dendritic extensions (N8) (Figure 1 – figure supplement 1A) and robust

24   upregulation of several classical neuronal markers including, TrkB, MAP2 and

25   TUBB3 (NPC and N8), while stem cell pluripotency marker Nanog became

8

1   significantly reduced upon differentiation (Figure 1 – figure supplement 1B).

2   Using available circRNA prediction tools CIRI2 (Gao, Zhang, & Zhao, 2018),

3   find_circ (Memczak et al., 2013) and CIRCexplorer2 (Zhang et al., 2016) on the

4   non-RNase R-treated RNA, we identified between 792-1167 circRNAs in

5   mESC, 2230-2893 circRNAs in NPC and 1902-2316 circRNAs in differentiated

6   neurons at N8 stage (Figure 1B). Upon RNase R treatment most circRNAs

7   either remained unchanged or became enriched, but a considerable fraction of

8   the predicted circRNAs in mESC, mNPC and mN8 preparations, became

9   depleted by the 3'-5' exonuclease (CIRCexplorer2: 19.5-36.5%; CIRI2: 7.2-

10   16.6%; find_circ: 38.7-52.3% depleted) (Figure 1 – figure supplement 1C). All

11   prediction algorthims showed a correlation between expression level and

12   RNase R resistance, suggesting that mostly low-count circRNAs candidates

13   are likely false positives (Figure 1 – figure supplement 1D). From a total of 3581

14   enriched circRNAs after RNase R treatment (all stages), 1449 circRNAs

15   overlapped between all 3 circRNA prediction algorithms, and this subset

16   represents a high-confidence circRNA inventory (Hansen, Veno, Damgaard, &

17   Kjems, 2015) (Figure 1C and Table S1). We next assessed the *circular-to-linear*

18   ratio of identified circRNAs (find_circ), by comparing splice site usage in circular

19   vs. linear splicing events (Memczak et al., 2013; Rybak-Wolf et al., 2015). This

20   analysis revealed vast differences in the steady-state levels of these isoforms

21   and demonstrated that many circRNA species are considerably more abundant

22   than their linear precursors (Figure 1D). Confirming previous results (Rybak-

23   Wolf et al., 2015), introns flanking the circRNAs are generally longer than

24   average introns and circRNAs often tend to cluster at the 5' end of their

25   respective precursor RNA (Figure 1 – figure supplement 1E-F). Our results

1 suggest that in order to obtain high confidence circRNA inventories from RNA-

2 seq data, it is beneficial to use multiple circRNA prediction algorithms and to

3 enrich for bona fide circRNAs, by depletion of linear RNAs using RNase R.

4 We next tested differential circRNA expression during differentiation, which

5 revealed marked changes in circRNA expression over the 16-day timecourse

6 (Figure 1E; left panel). Kmeans clustering of circRNAs by expression (Top 100

7 highest expressed) pattern showed two main clusters with peak expression at

8 mNPC and mN8 (Figure 1E; right panel). Comparison with previously identified

9 mouse and human homologue circRNAs, isolated from mouse brain regions or

10 cell lines of either murine or human origin (Rybak-Wolf et al., 2015), revealed

11 significant overlap between circRNAs at differentiated stages (e.g. 80% of all

12 1449 circRNAs found in differentiated murine p19 cells and primary neurons,

13 45% of Top100 found in human SH-SY5Y and 75% overlap with circRNAs

14 found in the human ENCODE data previously analysed (Rybak-Wolf et al.,

15 2015; Stagsted et al., 2019)) (Figure 1 – figure supplement 1G). We confirmed

16 differential expression of a subset of the most abundant and upregulated

17 circRNAs (circTULP4, circMAGI, circRMST, circEZH2, circHDGFRP3,

18 circZFP827, circMEDL13, circZFP609, circSLC8A1, circNFIX) using RT-qPCR

19 with amplicons across the backsplicing junction (Figure 1F-G). 75% of the top-

20 100 expressed mouse circRNAs was also found in human circRNA datasets

21 (Rybak-Wolf et al., 2015) (Figure 1 – figure supplement 1G). We conclude that

22 significant changes in circRNA expression patterns are induced upon neuronal

23 differentiation and that the majority of these circRNAs are conserved between

24 various neuronal cell-types originating from humans and the mouse.

25

1   *Knockdown of circZNF827 stimulates neuronal marker expression*

2   To ascertain whether the highly upregulated circRNAs might contribute to the

3   process of neuronal differentiation, we next depleted a number of candidate

4   circRNAs by RNA interference. We first tested knockdown efficiency of

5   circZfp827 (circZNF827 in humans) by lentivirally delivered dishRNAs (Kaadt

6   et al., 2019) targeting the backsplicing junction in either mESC, p19, SH-SY5Y

7   or L-AN-5 cells, of which the latter three cell lines are well established models

8   of neuronal differentiation following retinoic acid treatment. Knockdown

9   efficiency in mESC and p19 proved relatively poor (30-60% remaining circRNA)

10   compared to the two human cell lines: SH-SY5Y (10% remaining) and L-AN-5,

11   which displayed superior results (<8% remaining) (Figure 2A and Figure 2 –

12   figure supplement 1A). Moreover, when testing SH-SY5Y cells for an increase

13   of neuronal differentiation markers *TrkB*, *NEFL*, *MAP2* and *TUBB3* upon

14   retinoic acid treatment, only *TrkB* was significantly upregulated upon

15   differentiation (Figure 2 – figure supplement 1B), whereas these genes showed

16   a more expected and dynamic expression pattern in L-AN-5 cells (Figure 2B).

17   We therefore transduced L-AN-5 cells with lentiviral dishRNA vectors to

18   perform knockdown of 14 candidate circRNAs (Figure 2 – figure supplement

19   1C; circTULP4, circSLC8A1, circZNF609, circHDGFRP3, circMAGI, circRMST,

20   circZNF827, circANKIb, circMED13L, circCDYL, circUNC79, circHIPK3,

21   circNFIX, circCAMSAP1) (Table S2) and subsequently subjected these to

22   retinoic acid-induced differentiation followed by neuronal marker quantification

23   in order to probe for changes in differentiation. In general, we observed efficient

24   knockdown (Figure 2A and Figure 2 – figure supplement 1C). While the majority

25   of knockdowns did not significantly change neuronal marker expression,

11

1   knockdown of circZNF827 (and to a lesser extent circANKIb), produced a

2   significant and reproducible increase in neuronal marker expression upon

3   differentiation (Figure 2B and Figure 2 – figure supplement 2A). Importantly,

4   the linear *ZNF827* mRNA was not affected by backsplicing junction-specific

5   knockdown (Figure 2 – figure supplement 2B). The upregulation of neuronal

6   markers following circZNF827 knockdown was also evident at the protein level

7   for MAP2 and TUBB3 (Figure 2C, and quantified to the right). In addition,

8   proliferation assays demonstrated a smaller S-phase population (32% to 24%)

9   upon circZNF827 knockdown, suggesting lowered replication kinetics (Figure

10   2D and Figure 2 – figure supplement 3A-B). This phenomenon was

11   accompanied by a minor stall in G_2/M phase, while G_0/G_1 phase was not

12   significantly affected between control and circZNF827 knockdown. Taken

13   together, our results suggest that circZNF827 exerts a repressive effect on

14   proliferation, neuronal marker expression and hence differentiation.

15

16   *circZNF827 controls retinoic acid receptor homeostasis*

17   We next asked whether the Retinoic Acid Receptors (RARs), which represent

18   central nodes in relaying anti-proliferative differentiation cues during neuronal

19   development (Gudas & Wagner, 2011), and are key targets of retinoic acid,

20   also become upregulated upon knockdown of circZNF827. Indeed, knockdown

21   of circZNF827 leads to a moderate but significant increased expression (1.5-

22   2.5 fold) of $RAR\alpha$ and $RAR\gamma$, while $RAR\beta$ remained constant (Figure 3A). Since

23   most circRNAs have been reported to predominantly localize in the cell

24   cytoplasm, we addressed the localization of circZNF827, circANKIb and

25   circTULP4 by cellular fractionation. These circRNAs are mainly cytoplasmically

1   localized in L-AN-5 cells (~90% cytoplasmic signal) (Figure 3B). We therefore

2   hypothesized that circZNF827 could potentially affect *RAR*-mRNA stability

3   post-transcriptionally in the cell cytoplasm. However, BrU pulse-chase mRNA

4   decay assays demonstrated no significant change in *RAR*-mRNA decay rates

5   upon knockdown of circZNF827 (Figure 3C). Next, we investigated transcription

6   rates, by treating cells with a short pulse of BrU, followed by BrU

7   immunoprecipitation to quantify *de novo* labeled RNA, serving as a proxy for

8   transcription rates during control- or knockdown of circZNF827. As expected

9   from the constant mRNA decay rates, BrU incorporation was upregulated, upon

10   circZNF827 knockdown (Figure 3 – figure supplement 1). Our results suggest

11   that circZNF827 contributes to controlling RA-receptors transcriptionally, in

12   order to keep neuronal differentiation in check.

13

14   *circZNF827 knockdown affect multiple genes in neuronal signaling*

15   Our results indicate that L-AN-5 cells are lowering their proliferation rates and

16   promote RAR-signalling by transcriptional upregulation of these transcription

17   factors when circZNF827 levels are low. To test how circZNF827 knockdown

18   affects other key factors of the neuronal transcriptome, we next performed

19   Nanostring analyses using a neuro-differentiation/pathology panel of 760 genes

20   with RNA purified from differentiated or non-differentiated L-AN-5 cells. 135

21   genes become differentially expressed (9 upregulated and 126 downregulated,

22   fold change > +/-2, p<0.05) due to circZNF827 knockdown after differentiation

23   (Figure 4A, Table S3). In line with a potential negative regulatory function of

24   circZNF827 on neuronal differentiation, GO-term analyses show enrichment of

25   terms including axon/dendrite structure, neural cytoskeleton, transmitter

1   synthesis, neural connectivity, growth factor signaling and trophic factors

2   among differentially expressed genes (Figure 4B). The most significantly

3   upregulated gene is nerve growth factor receptor (NGFR), which plays a central

4   role in regulating neuronal differentiation, death, survival and neurite outgrowth

5   (Yamashita, Tucker, & Barde, 1999; Zhu et al., 2012). Conversely,

6   Phosphatase and tensin homolog (PTEN), STAT3 and NAD(P)H quinone

7   dehydrogenase 1 (NQO1) were all significantly downregulated upon

8   circZNF827 knockdown (2-4 fold), which reportedly also contributes positively

9   to neuronal differentiation (Lyu et al., 2015; Ma, Zhou, Chai, Wang, & Huang,

10   2017), and in case of the latter, also renders cells more susceptible to energetic

11   and proteotoxic stress (Hyun et al., 2012). Since NGFR is a key regulator of

12   neuronal differentiation and the highest upregulated gene upon circZNF827

13   knockdown, we next focused on the mechanism of its upregulation. Using both

14   qRT-PCR and western blotting, which demonstrated a strong upregulation at

15   both the protein and mRNA level (Figure 4C and Figure 4 – figure supplement

16   1). This upregulation was not due to changes in mRNA decay rates, since BrU

17   pulse-chase mRNA decay assays yielded nearly identical mRNA half-lives

18   upon circZNF827 knockdown (Figure 4D). To address whether the observed

19   changes in gene expression are elicited at the transcriptional level, we

20   subjected cells to a short BrU-pulse prior to BrU immunoprecipitation and

21   Nanostring hybridization. Interestingly, NGFR and also ATP8A2 proved to be

22   highly upregulated (~4-6 fold) at the level of transcription (Figure 4E-F), while

23   only NQO1 and not PTEN and STAT3 exhibited significantly reduced

24   transcription activity (ranging from ~1.3 to ~4 fold) (Figure 4E). Also, the MAP2

25   gene did not change its *de novo* RNA output, suggesting that the tuning of the

14

1   steady-state levels of *PTEN*, *STAT3* and *MAP2* mRNAs, as initially observed

2   (Figure 2A and 4A), are mainly facilitated by posttranscriptional changes to

3   mRNA stability. If circZNF827 is involved in a *direct* transcription-associated

4   complex that regulates NGFR output, the transcriptional effects elicited by

5   circZNF827 knockdown would require nuclear knockdown of the circRNA.

6   Indeed, the use of dicer-independent shRNA (dishRNA) vectors proved very

7   efficient in depleting nuclear circRNA (Figure 4G).

8   Next, we assayed the cellular impact of *NGFR* upregulation upon circZNF827

9   knockdown. To this end, we NGF-treated L-AN-5 cells subjected to either

10   control or circZNF827 knockdown, and quantified downstream signaling output

11   by quantification of *c-fos*, which is a well-known downstream "immediate early"

12   target of NGFR signaling. *c-fos* levels increased significantly, strongly indicating

13   that the higher levels of NGFR protein indeed leads to functional increase in

14   NGFR signaling (Figure 4H), which can at least in part explain the upregulation

15   of neuronal markers. Taken together, we conclude that circZNF827 serves to

16   keep neuronal differentiation 'in check' by limiting expression of, and signaling

17   by, RARs and NGFR.

18

19   *circZNF827 interacts with transcriptional regulators hnRNP K and -L.*

20   To address the mechanism by which these transcriptional and post-

21   transcriptional events are controlled by circZNF827, we next sought to identify

22   its protein interactome. To this end, we synthesized biotin-labeled circZNF827

23   (linear version) and control RNAs (circTULP4, circZNF609, circHDGFRP3 and

24   circSLC8A1) *in vitro* and subjected these to pull-down experiments using L-AN-

25   5 cell lysates and streptavidin-coupled magnetic beads as previously described

1   (Seitz et al., 2017). Silver-stained SDS-PAGE gels of retained proteins revealed

2   unique profiles, suggesting that specific proteins exhibited increased affinity

3   towards circZNF827, although prominent RNA-binding proteins common to

4   both control RNAs and circZNF827 could also be observed (Figure S5A). By

5   subjecting pulled-down fractions to LC-MS/MS, we identified several

6   circZNF827-specific proteins, including hnRNP K and -L, while others (e.g.

7   DHX9 and DDX3X) bound strongly to any of the bait RNAs (Figure 5A). To

8   validate these interactions, we performed RNA-immunoprecipitaiton (RIP)

9   using monoclonal anti-hnRNP K or -L antibodies followed by qRT-PCR across

10   the backsplicing junction, and observed a significant enrichment of circZNF827

11   compared to IgG controls (~100-130 fold), suggesting that these interactions

12   can be recapitulated in L-AN-5 cells (Figure 5B). As expected for these highly

13   expressed RNA binding proteins, both proteins associate with GAPDH *mRNA*,

14   but in the case of hnRNP L, the IP/input ratios were ~18 fold higher for

15   circZNF827, whereas hnRNP K displayed a similar enrichment of *GAPDH*

16   mRNA as of circZNF827 (Figure 5B). Scrutinizing the circZNF827 sequence for

17   putative binding sites for hnRNP K and -L using eCLIP datasets (ENCODE

18   consortium), proved unfeasible due to low expression levels of the ZNF827

19   gene in the K562 and HepG2 cells used by ENCODE. Using RBPmap(Paz,

20   Kosti, Ares, Cline, & Mandel-Gutfreund, 2014), which is based on established

21   RBP consensus binding sequences, revealed a potential high affinity cluster for

22   primarily hnRNP L binding and one site for hnRNP K in the most 3' part of the

23   circle-encoding sequence (Figure 5 – figure supplement 1B-C). According to

24   circZNF827 secondary RNA structures predicted by Mfold, these binding sites

25   are located into mostly single stranded regions within the circRNA, consistent

1   with the binding preferences of most hnRNP proteins towards single stranded

2   RNA (Figure 5 – figure supplement 1D). To further characterize these

3   interactions we prepared a stable HEK293 Flp-In T-rex cell-line expressing

4   circZNF827 (Figure 5 – figure supplement 1E-F) under the control of a

5   tetracycline inducible promoter (tet-on), based on the laccase vector system

6   (Kramer et al., 2015). We then performed RIP by immunoprecipitation of

7   endogenous hnRNP K or -L and observed a remarkable enrichment of

8   exogenous circZNF827, compared to control IgG or *GAPDH* mRNA (Figure 5C

9   and E). hnRNP L gave a particularly high IP/Input ratio (~200 fold enrichment),

10   consistent with the results from: 1) the L-AN-5 RIP, 2) the pull-down LC-MS/MS

11   experiment and 3) the prediction of several hnRNP L binding site clusters in

12   circZNF827. We conclude that both hnRNP K and -L can be found in complex

13   with endogenous or exogenous circZNF827 in both L-AN-5 and HEK293 Flp-in

14   T-Rex cells.

15

16   *Increasing expression of circZNF827 induces distinct hnRNP K nuclear foci*

17   hnRNP K is a well-documented transcriptional regulator (Moumen, Masterson,

18   O'Connor, & Jackson, 2005; Thompson et al., 2015) that is reported to interact

19   directly with hnRNP L and -U (Havugimana et al., 2012; Kim, Hahm, Kim, Choi,

20   & Jang, 2000; Wan et al., 2015) and bind both DNA and RNA (Tomonaga &

21   Levens, 1995). To assess interactions between hnRNP K, -L and -U, and their

22   potential dependence on circZNF827, we performed co-immunoprecipitation

23   experiments using FLAG-tagged hnRNP K, -L and -U, and subsequently

24   probed for their interaction with endogenous proteins (Figure 5D) in HEK293

25   cells   either   overexpressing   circZNF827   or   not.   hnRNP   K   co-

1   immunoprecipitates both hnRNP U and hnRNP L (long isoform), but these

2   interactions remain unaffected by increased expression of circZNF827 (Figure

3   5D). In accordance with these findings, immunoprecipitation of endogenous

4   hnRNP K and -L proteins in HEK293 Flp-in cells, with or without laccase-driven

5   overexpression of circZNF827, confirmed that a hnRNP L/ hnRNP K complex

6   can indeed be detected (Figure 5E, left), and that this complex is not affected

7   by expression of circZNF827 (Figure 5E, right). Hence, circZNF827 likely does

8   not regulate bulk hnRNP K/L-complex assembly/disassembly *per se*.

9   To test whether circZNF827 potentially regulate the normal subcellular

10   distribution of hnRNP K, L-AN-5 cells were fractionated during control or

11   circZNF827 knockdown and lysates subjected to western blotting. We observe

12   a small but significant and reproducible increase in the cytoplasmic population

13   of hnRNP K upon circZNF827 knockdown, suggesting that circZNF827 retains,

14   albeit a very small fraction of the hnRNP K population, in the nucleus (Figure

15   5F). To address this, we overexpressed circZNF827 and monitored hnRNP K

16   and L localization by immunofluorescence in HEK293 cells. Induction of

17   circZNF827 led to accumulation of hnRNP K and to a lesser extent hnRNP L in

18   multiple distinct nuclear foci that were not detected in control cells (Figure 5G).

19   Taken together, our results suggest that while bulk hnRNP K and L complex

20   formation is not affected by circZNF827 levels, overexpression of the circRNA

21   induces specific nuclear localization of hnRNP K and L.

22

23   *hnRNP K or -L knockdown enhances NGFR levels by increasing RNA-Pol*II

24   *engagement on the NGFR gene*

1   Could a circZNF827-dependent hnRNP K/L-containing nuclear complex

2   regulate the output from the NGFR gene? If such a complex is instrumental in

3   repressing NGFR, we predict that knockdown of any of these factors would

4   enhance NGFR expression. In support of a role in hnRNP K-mediated

5   regulation of NGFR, it was recently reported that hnRNP K knockdown strongly

6   induces NGFR expression in mouse ES cells (Thompson et al., 2015). To test

7   this in our context, we designed dishRNAs for hnRNP K and -L, transduced L-

8   AN-5 cells and assayed for NGFR expression by qRT-PCR or Western blotting.

9   Both knockdowns increased NGFR expression at both the mRNA and protein

10   levels, similar to the effect of depleting circZNF827 alone (Figure 6A-B and

11   Figure 6 – figure supplement 1A-B). However, co-depletion of circZNF827 with

12   any of these factors strongly augmented NGFR expression (4-5 fold higher than

13   individual knockdowns) (Figure 6A-B), suggesting that their effects are

14   synergistic.

15   Given these results, a feasible possibility is that a hnRNP K/L-circZNF827

16   complex could facilitate transcriptional repression of NGFR by interacting with

17   gene-regulatory regions, consistent with NGFR upregulation upon circZNF827

18   knockdown. To this end, publicly available ChIP-seq data (ENCODE

19   consortium) in K562 and HepG2 cells demonstrate that hnRNP K indeed

20   interacts with transcription regulatory regions (promoter proximal) of the NGFR

21   gene (Figure 6 – figure supplement 1C). To determine the circZNF827-

22   dependence of a hnRNP K-containing complex that docks at the promoter

23   region of NGFR gene in L-AN-5 cells, we next performed hnRNP K and RNA

24   PolII ChIP in the presence or absence of circZNF827 and assayed for the

25   NGFR promoter region by qPCR. Our results show that RNA-PolII engagement

19

1   is increased at the NGFR promoter, while hnRNP K engagement is decreased

2   upon circZNF827 knockdown compared to the GAPDH gene (Figure 6C), which

3   displayed constant transcription rates in our previous BrU pulse labeling assay.

4   We next wondered how this circRNP complex can interact with chromatin. It

5   was recently demonstrated that hnRNP K partakes in a complex with

6   chromatin-bound KRAB-domain zinc finger proteins (KRAB-ZNFs), and that

7   hnRNP K is necessary for recruitment of a transcription inhibitory

8   SETDB1/KAP1 complex, which catalyzes H3K27 trimethylation and

9   heterochromatin formation (Thompson et al., 2015). We therefore hypothesized

10   that ZNF827 protein, which does not harbor a discernible KRAB domain, could

11   interact with either hnRNP K and/or its encoded circRNA and perhaps link this

12   complex to the NGFR promoter. To this end, we performed ZNF827

13   immunoprecipitation and found it to strongly associate with hnRNP K and to a

14   lesser extent with hnRNP L in nucleoplasmic extracts (Figure 6D, left). Upon

15   sonication of the remainder from the Triton X-100 extracted cleared lysates

16   (chromatin enriched), we observed an even stronger association of hnRNP K

17   with ZNF827, suggesting that the complex is chromatin bound (Figure 6D,

18   right). When assessing the ability of ZNF827 to interact with circZNF827, we

19   observed a strong enrichment over IgG (~18 fold), and ZNF827 protein co-

20   immunoprecipitated circZNF827 more efficiently than *GAPDH* (~19 fold more

21   enriched) (Figure 6E).

22   Taken together, our results are consistent with a model where circZNF827

23   represses NGFR transcription (and likely many other genes) by bridging a

24   hnRNP K/L-contaning inhibitory complex with their genomic loci, possibly

25   facilitated by the ZNF827 protein, which in turn contributes to keeping an

1 important balance between neuronal differentiation and self-

2 renewal/proliferation in L-AN-5 cells (Figure 7).

3

4 **Discussion**

5

6 Circular RNAs are by now considered as an important class of abundant and

7 conserved RNAs but their functional potential has not been fully elucidated yet.

8 Here, we identified high-confidence circRNA inventories of E14 mESCs, NPCs

9 and differentiated glutamatergic neurons, and show a generally high degree of

10 conservation among circRNAs previously identified using cell lines and tissues

11 of neuronal origin (Rybak-Wolf et al., 2015). Three different circRNA prediction

12 pipelines, CIRI2 (Gao et al., 2018), find_circ (Memczak et al., 2013) and

13 CIRCexplorer2 (Zhang et al., 2016), displayed marked differences in their

14 predictions, which is in line with our earlier observations(Hansen et al., 2016).

15 This could indicate that many reported circRNAs are false positives, especially

16 when expressed at low levels. A surprisingly large fraction of initially called

17 circRNAs by the three pipelines becomes depleted upon RNase R treatment

18 (between 7,2% and 52,3%), with CIRI2 clearly being the most robustly

19 performing predictor in terms of RNase R resistance. Among 3581 RNase R-

20 resistant circRNAs, only 1449 were called by all three algorithms, suggesting

21 that caution should be taken when predicting circRNAs from RNA-seq data and

22 that including multiple prediction algorithms and/or an RNase R step prior to

23 RNA-seq is beneficial.

24 Analyzing circRNA expression over the three neuronal developmental stages,

25 we identified 116 differentially expressed circRNAs (>2-fold change). Of 14

21

1 tested circRNA candidates, knockdown of circZNF827 in human L-AN-5 cells

2 had a significant and positive impact on the expression of several classical

3 neuronal markers, suggesting that the circRNA normally exerts a negative role

4 in neuronal differentiation. Among 760 genes important to neuronal

5 differentiation and disease, we found that NGFR was most strongly induced,

6 also at the protein level, upon circZNF827 knockdown. NGFR is a member of

7 the TNF superfamily of receptors and relays, along with three paralogous

8 receptor tyrosine kinases (TrkA, TrkB and TrkC), signals from the 4 mammalian

9 neurotrophins (Nerve Growth Factor (NGF), brain-derived neurotrophic factor

10 (BDNF), neurotrophin-3 (NT-3) and neurotrophin 4 (NT-4, aka. NT-4/5)

11 (Bothwell, 2016). The regulation and functional output from the neurotrophins

12 and their receptors, which are interdependent proteins, is very complex and

13 involves a multitude of effector proteins and interaction partners(Bothwell,

14 2016). NGFR can, depending on expression levels of the other neurotrophin

15 receptors and their ligands, either induce death- or survival signaling to promote

16 neuronal differentiation and control axonal growth or apoptosis (Bothwell,

17 2016). Whether NGFR upregulation is instrumental and causal for the

18 enhanced expression of TrkB, NEFL, TUBB3 and MAP2 that we observe in the

19 L-AN-5 neuroblastoma system, remains to be investigated. However, we did

20 observe strongly augmented c-fos expression (immediate early gene) upon

21 treatment of L-AN-5 cells with NGF, when circZNF827 was downregulated,

22 which suggests that TrkA-mediated NGF response becomes enhanced by

23 increased NGFR expression. It is possible that NGFR is induced to increase

24 death-signalling, as a result of skewed and sub-optimal stoichiometry between

25 key neuronal markers/effectors (e.g. TrkB, NEFL, TUBB3 and MAP2). Such a

22

1 scenario might be part of a normal surveillance system that monitors a strict

2 and sequential appearance of differentiation factors, however, this awaits

3 further disclosure in more physiologically relevant cell- and animal models.

4

5 Mechanistically, several lines of evidence support a model in which circZNF827

6 plays a direct role in the transcriptional repression of the NGFR locus,

7 potentially as a scaffolding-RNA for a hnRNP K-containing complex (Figure 7).

8 *NGFR* mRNA decay rates remain unchanged upon circZNF827 knockdown,

9 while stready-state levels increase 3-4 fold. Knockdown of circZNF287 resulted

10 in significantly higher BrU incorporation rates in *NGFR* pre-mRNA and an

11 increased association of PolII at the NGFR promoter. Importantly, hnRNP K

12 association with the NGFR promoter was decreased upon circZNF287

13 knockdown. In addition, depletion of either hnRNP K or -L, which both interact

14 robustly with circZNF827, strongly augmented the transcriptional induction by

15 circZNF827 knockdown. We observed strong focal nuclear condensates

16 containing endogenous hnRNP K and -L proteins in HEK293 Flp-in T-Rex cells

17 stably expressing circZNF827. Although such condensates may be non-

18 physiological entities (phase-separated hnRNPs), induced by high local

19 concentrations of circZNF827, these results suggest that the circRNA could

20 function as a scaffold that nucleates hnRNP K and -L, although not readily

21 visible in the microscope when circZNF827 levels are significantly lower.

22 It is well established that hnRNP K participates in transcriptional repression.

23 hnRNP K can bridge classical DNA-binding KRAB-ZNF proteins and a

24 KAP1/SETDB1-containing complex, which in turn facilitates heterochromatin

25 formation – also in the NGFR gene of ES cells (Thompson et al., 2015). A

23

1   similar mechanism was described by Huarte and collegues, where a p53-

2   induced lincRNA-p21 interacts with hnRNPK, which facilitates silencing of

3   several downstream targets (Huarte et al., 2010). Interestingly, transcriptional

4   stimulation, rather than repression, has been reported for intron-containing

5   circRNAs (ElciRNAs), via recruitment of U1 snRNP to the transcriptional

6   complex on their parental genes, which by definition requires exon-intron

7   boundaries (Li et al., 2015). CircZNF827 is a regular exonic circRNA, without

8   intronic sequences (data not shown), perhaps explaining why it represses

9   transcription as opposed to ElciRNAs. Another circRNA, circSLC45A4, was

10   recently also shown to negatively regulate neuronal differentiation, both in cell

11   cultures and in developing mice, where its knockdown dysregulates the balance

12   between specialized cortex neurons (Suenkel et al., 2020). How transcription

13   regulatory factors are recruited to the NGFR promoter (and likely others in the

14   genome) by this circZNF827-hnRNPK/L complex, remains unknown, but our

15   finding that hnRNP K can interact with ZNF827 protein, which is a DNA-binding

16   protein, suggest that the protein encoded by the circZNF827 precursor mRNA,

17   may play a yet undefined role in this phenomenon. If so, circZNF827 co-

18   regulates target genes along with its precursor-encoded protein, which argues

19   for co-evolutionary selection pressure to preserve both circRNA-generating and

20   protein-coding sequences. circMBNL1 has also been shown to regulate the

21   activity of its cognate protein product (Ashwal-Fluss et al., 2014), suggesting

22   that this phenomenon could be a common theme that awaits further

23   investigation.

24

25   **Materials and Methods**

1

2   Sequences of all primers and probes used in the study are specified in Table

3   S4. Antibodies are described in Table S5.

4

5   *Vector construction*

6   To create plasmids for expression of dishRNAs, sense and antisense

7   oligonucleotides were annealed and cloned into BglII/XhoI-digested pFRT/U6,

8   resulting in vectors designated pFRT/U6-dishRNA(Kaadt et al., 2019).

9   Subsequently, the U6-dishRNA expression cassettes were PCR-amplified from

10   pFRT/U6-dishRNA vectors and inserted into ClaI/BsiWI-digested pCCL/PGK-

11   eGFP-MCS(Kaadt et al., 2019). The resulting lentiviral transfer vectors were

12   designated pCCL/U6-dishRNA-PGK-eGFP-MCS.

13   To generate plasmids for in vitro transcription of circRNAs, the exons encoding

14   circTULP4, circZNF827, circHDGFRP3, circZNF609, and circSLC8A1 were

15   PCR-amplified from cDNA prepared from RNA isolated from L-AN-5 cells.

16   PCR-amplicons encoding circTULP4, circZNF827, circHDGFRP3, and

17   circSLC8A1 were inserted in BamHI/NotI-digested pcDNA3/PL whereas PCR-

18   amplicons encoding circZNF609 were inserted in HindIII/NotI-digested

19   pcDNA3/PL. The resulting plasmids were designated pcDNA3/circRNA. The

20   plasmid for expression of the CTC lincRNA was constructed as previously

21   described in (Seitz et al., 2017).

22   For exogenous expression of circZNF827, the exons encoding circZNF827

23   were PCR-amplified from cDNA prepared from RNA isolated from L-AN-5 cells

24   and inserted into PacI/SacII-digested pcDNA3.1(+)-Laccase2-MCS-exon-

25   vector (Kramer et al., 2015). Subsequently, the Laccase-circZNF827

1   expression cassette was inserted into HindIII/NotI-digested pcDNA5_FRT/TO

2   resulting in a vector designated pcDNA5_FRT/TO-Laccase2-circZNF827.

3   To create plasmids for expression of FLAG-tagged RNA binding proteins

4   (RBPs), the coding sequences of RBPs hnRNPK, hnRNPL, hnRNPU, DDX3X,

5   and DHX9 were PCR-amplified from cDNA prepared from RNA isolated from

6   L-AN-5 cells whereas eGFP was sub-cloned from pNEGFP (HindIII/HindIII) and

7   inserted into either KpnI/NotI-, BamHI/NotI- or HindIII-digested

8   pcDNA5_FRT/TO-FLAG. The resulting plasmids were designated

9   pcDNA5_FRT/TO-FLAG-RBP. All plasmids were verified by Sanger

10   sequencing.

11

12   *Cell culturing*

13   L-AN-5 cells were maintained in RPMI whereas SH-SY5Y and HEK293T cells

14   were maintained in DMEM medium (Gibco, Dublin, Ireland, 32430100). For all

15   three cell lines the cell culture medium was supplemented with 10% fetal bovine

16   serum (Gibco, 10082139) and 1% penicillin/streptomycin (Gibco, 15140122).

17   P19 cells were maintained in MEMα supplemented with 7.5% newborn calf

18   serum (Gibco, 26010074), 2.5% fetal bovine serum (Gibco, 10082139), and 1%

19   penicillin/streptomycin (Gibco, 15140122). HEK293 Flp-In T-Rex cells were

20   maintained in DMEM supplemented with 10% tetracyclin-free fetal bovine

21   serum (Gibco, 10082139) and 1% penicillin/streptomycin (Gibco, 15140122).

22   All cells were cultured at 37°C in 5% (v/v) CO_2.

23   For neuronal differentiation of the neuroblastoma cell lines L-AN-5, SH-SY5Y,

24   and P19 10 μM retinoic acid (RA) (Sigma-Aldrich, St. Louis, Missouri, United

25   States) was added to the cell culture medium for four days.

1   The cell line with stable expression of circZNF827 was generated as previously

2   described (Hollensen et al., 2018). Briefly, HEK293 Flp-In T-Rex cells were co-

3   transfected with pcDNA5-FRT/TO-laccase2-circZNF827 and a plasmid for

4   expression of the Flp recombinase (pOG44). Cell culture medium

5   supplemented with 100 ng/ml Hygromycin (Thermo Scientific, Waltham,

6   Massachusetts, United States) and 10 ng/ml Basticidin S (Thermo Scientific)

7   was used for selection of positive clones. The resulting cell line was designated

8   HEK293 Flp-In T-Rex circZNF827. Tetracycline (Tet) concentrations used for

9   titration of circRNA induction (Northern blot) were 5 ng/ml, 25 ng/ml, 100 ng/ml

10   and 250 ng/ml, respectively. 25 ng/ml Tet was used for RIP experiments and

11   250 ng/ml Tet for hnRNP K/L immunofluorescence assays.

12

13   *mESC culture and differentiation*

14   E14 mESCs were grown on 0.1% gelatin coated plates in 2i medium(Ying et

15   al., 2008) containing: DMEM/F12 (Gibco, 31331) and Neurobasal (Gibco,

16   12348) 1:1, N2 supplement (Gibco, 17502048), B27 supplement (Gibco,

17   17504044), 1X glutaMax (Gibco, 35050061), 1X penicilin/streptomycin (Gibco,

18   15140122), 1 mM sodium pyruvate (Gibco, 11360070), 50 nM 2-

19   mercaptoethanol (Gibco, 31350010), nonessential amino acids (Gibco,

20   11140076), LIF, 3 µM GSK3 inhibitor (CHIR-99021) and 1 µM MEK inhibitor

21   (PD0325901). They were differentiated into neurons as previously described

22   (Bibel et al., 2007) with some modifications. 4 million cells were differentiated

23   into embryoid bodies in suspension in petri dishes for bacterial culture in 15ml

24   medium containing the same as before, but with 10% FBS and without LIF or

25   GSK3 and MEK inhibitors. Every second day, the medium was changed and

1   the embryoid bodies transferred to fresh petri dishes. On days 4 and 6, 5 µM

2   ATRA (Sigma-Aldrich, R2625) was added to the medium. On day 8 of

3   differentiation, the embryoid bodies were disgregated with 5% trypsin (Gibco,

4   15400054) and the cells plated in poly-DL-ornithine (Sigma-Aldrich, P8638) and

5   laminin (Sigma-Aldrich, L2020) coated plates in N2 medium, containing

6   DMEM/F12 and neurobasal 1:1, N2 supplement, sodium pyruvate, glutaMax,

7   15 nM 2-mercaptoethanol, and 50 µg/ml BSA. The medium was changed after

8   2 h and after 24 h. 48 h after plating the neuronal precursors, the medium was

9   changed to complete medium, containing B27 supplement, in addition to the

10   N2 medium. Neurons were harvested 2 and 8 days after plating.

11

12   *RNA sequencing and circRNA prediction*

13   20 µg RNA from each sample was depleted of rRNA using a Ribo-Zero rRNA

14   Magnetic Kit (Epicentre, St Louis, Missouri, United States) including the

15   optional RiboGuard RNase inhibitor according to the manufacturer's protocol.

16   The concentration was normalised so that each sample contained the same

17   amount of RNA. To 1/3 of the sample 1/10 of the recommended amount of

18   spike-in (ERCC RNA spike-in mix, Ambion) was added, ethanol precipitated,

19   and resuspended in 'Elute, fragment, finish mix' (Illumina, San Diego,

20   California, United States). The remaining 2/3 of the sample was ethanol

21   precipitated and resuspended in 15 µl nuclease free water. The sample was

22   heated to 70˚C for 1 min and incubated on ice for 2 min. 5 µl RNase R mixture

23   (Epicentre) was added to the sample before incubation at 37˚C for 30 min.

24   RNase R was removed by phenol/chloroform extraction. The RNA was

25   resuspended in 'Elute, fragment, finish mix' (Illumina). Sequencing libraries

1 were prepared using Truseq stranded RNA LT kit (Illumina) from both Ribo-

2 Zero and Ribo-Zero/RNase R samples, by fragmentation, 1st and 2nd strand

3 cDNA synthesis, 3'-end adenylation, ligation of adaptors, and enrichment of

4 DNA fragments using the manufacturer's protocol. The quality of the library was

5 validated using an Agilent Bioanalyzer 1000 (Agilent Technologies, Santa

6 Clara, California, United States). The samples were sequenced using the

7 Illumina HiSeq 2500 platform with 100 bp paired-end reads (AROS Applied

8 Biotechnology, Aarhus, Denmark).

9 Reads were mapped onto the mm10 genome, and circRNAs were detected and

10 quantified using find_circ (Memczak et al., 2013), CIRCexplorer2 (Zhang et al.,

11 2016) (v2.3.3), and ciri2 (Gao et al., 2018) (v2.0.6) using default settings except

12 for find_circ, where a stringent mapq threshold of 40 was used for both adaptor

13 sequences as proposed previously (Hansen, 2018). The prediction-output from

14 all pipelines was merged and intersected, and only circRNAs detected by all

15 three pipelines and with three-fold enrichment of backsplice-spanning reads in

16 the RNAseR treated samples were defined as bona fide. Expression, based on

17 untreated samples quantified ciri2, was RPM normalized and the top100

18 expressed bona fide circRNAs across all samples were subjected to kmean

19 clustering using five centers based on within-clusters sum of squared.

20 Annotated genes (UCSC annotation) with at least one splice site in common

21 with circRNAs were denoted as host genes, and based on host-gene

22 annotation, exon numbers and flanking intron lengths were extracted.

23 The circ-to-linear ratios were based on the backsplice junction spanning reads

24 and the mean of upstream and downstream linear spliced reads as quantified

25 by find_circ.

1   To compare with human expression profiles, the top100 expressed circRNAs

2   were converted from mm10 to hg19 coordinates using liftOver (UCSC), and

3   only fully matched loci were considered homologous.

4   RNAseq from Rybak-Wolf et al (GSE65926 (Rybak-Wolf et al., 2015)) was

5   solely analysed with find_circ using stringent settings as described above.

6

7   *Lentiviral production*

8   Third-generation lentiviral vectors were produced in HEK293T cells as

9   previously described(Hollensen et al., 2017). One day before transfection, cells

10   were seeded in 10-cm dishes at a density of 4×10^6 cells/dish. Transfections

11   were carried out with 3.75 µg pMD.2G, 3 µg pRSV-Rev, 13 µg pMDLg/pRRE

12   and 13 µg lentiviral transfer vector using a standard calcium phosphate or

13   polyethylenimine transfection protocol. Medium was changed to RPMI medium

14   one day after transfection. Two days after transfection viral supernatants were

15   harvested and filtered through 0.45 µm filters (Sartorius, Göttingen, Germany).

16   All lentiviral preparations were made in at least triplicates and pooled before

17   determination of viral titers. To determine viral titers of lentiviral preparations,

18   flow cytometric measurements of eGFP expression were used as previously

19   described(Hollensen et al., 2017). One day prior to transduction, L-AN-5 cells

20   were seeded at a density of 5×10^5 cells/well in 12-well plates. For all lentiviral

21   preparations, transductions with 10^2- and 10^3-fold dilutions of virus-containing

22   supernatants were carried out. Both viral supernatants and growth medium

23   were supplemented with 4 µg/ml polybrene. One day after transduction,

24   medium was changed. Five days after transduction, cells were harvested and

25   fixated in 4% paraformaldehyde (Sigma-Aldrich). eGFP expression levels were

1   analyzed on a CytoFLEX flow cytometer (Beckman Coulter, Brea, California,

2   United States). Lentiviral titers were calculated based on samples with between

3   1% and 20% eGFP positive cells using the formula: titer (TU/ml) = $F \cdot C_n \cdot DF/V$,

4   where F represents the frequency of eGFP positive cells, C_n the total number

5   of target cells counted the day the transductions were carried out, DF the

6   dilution factor of the virus and V the volume of transducing inoculum.

7

8   *circRNA knockdown and differentiation of L-AN-5 cells*

9   One day prior to transduction with lentiviral vectors encoding circRNA-specific

10   dishRNAs, L-AN-5 cells were seeded at a density of 6.6×10^6 cells/dish in 10-

11   cm dishes, 2.2×10^6 cells/dish in 6-cm dishes, or 0.8×10^6 cells/well in 6-well

12   plates. Transductions were carried out using equal MOIs calculated based on

13   titers determined by flow cytometry. Both viral supernatants and growth

14   medium were supplemented with 4 μg/ml polybrene. One day after

15   transduction, medium was changed. Two days after transduction, differentiation

16   was initiated by addition of 10 μM RA (Sigma-Aldrich) to the cell culture

17   medium. The L-AN-5 cells were differentiated for four days.

18

19   *NGF stimulation*

20   Lentiviral transduction and RA-mediated differentiation of L-AN-5 cells were

21   carried out as described in the section 'circRNA knockdown and differentiation

22   of L-AN-5 cells'. After four days of differentiation, the L-AN-5 cells were

23   stimulated with NGF (200 ng/ml) (Thermo Scientific) for 30 min and

24   subsequently harvested for RNA and protein purification.

25

1   *mRNA decay assay*

2   Lentiviral transduction and RA-mediated differentiation of L-AN-5 cells were

3   carried out as described in the section 'circRNA knockdown and differentiation

4   of L-AN-5 cells'. The L-AN-5 cells were cultured in 6-cm dishes containing 6 ml

5   cell culture medium supplemented with 10 μM RA. 4 ml cell culture medium

6   was aspirated from each 6-cm dish and pooled from cells transduced with the

7   same dishRNA. For one dish per dishRNA, the residual medium was aspirated

8   and 3.5 ml of the collected medium was added. For the remaining dishes, the

9   residual medium was aspirated and 3.5 ml of the collected medium

10   supplemented with 2 mM BrU (ThermoFisher) was added. 1 hour after addition

11   of BrU to the cell culture medium, the cells were washed three times in cell

12   culture medium. 50 min after removal of the BrU-containing cell culture medium

13   the first samples including the samples not treated with BrU were harvested.

14   Subsequently, samples were harvested after 3, 6 and 9 hours. Total RNA was

15   purified using 1 ml TRI Reagent (Sigma-Aldrich) according to manufacturer's

16   protocol. circRNA knockdown and differentiation of L-AN-5 cells were verified

17   by RT-qPCR using total RNA as described in the section 'Quantitative PCR'.

18   BrU-labeled RNA was immunoprecipitated as described elsewhere(Meola et

19   al., 2016). Briefly, BrU antibodies were conjugated to magnetic beads. 15 μl

20   Dynabeads M-280 Sheep Anti-Mouse IgG (Invitrogen, Carlsbad, California,

21   United States) per sample were washed twice in 1x BrU-IP buffer (20 mM Tris-

22   HCl (pH 7.5), 250 mM NaCl, 0.5 μg/μl BSA, 20 U/ml RiboLock (Fermentas,

23   Waltham, Massachusetts, United States) and resuspended in 1 ml 1x BrU-IP

24   buffer with heparin (20 mM Tris-HCl (pH 7.5), 250 mM NaCl, 1 mg/ml heparin).

25   After 30 min of incubation at room temperature on a rotator the beads were

1   washed in 1x BrU-IP buffer. Subsequently, the beads were resuspended in 1

2   ml 1x BrU-IP buffer supplemented with 0.9 µl mouse BrdU antibody (BD

3   Biosciences, San Jose, California, United States, clone 3D4) per sample and

4   incubated for 1 hour at room temperature on a rotator. The beads were washed

5   three times in 1x BrU-IP buffer and resuspended in 50 µl 1x BrU-IP buffer

6   supplemented with 1 mM 5-BrU per sample. After 30 min of incubation at room

7   temperature on a rotator the beads were washed three times in 1x BrU-IP buffer

8   and resuspended in 50 µl 1x BrU-IP buffer per sample. 25 µg of total RNA was

9   diluted to 200 µl and incubated at 80°C for 2 min. 200 µl 2x BrU-IP buffer with

10   BSA and RiboLock (20 mM Tris-HCl (pH 7.5), 250 mM NaCl, 1 µg/µl BSA, 80

11   U/ml RiboLock (Thermo Scientific) and 50 µl beads conjugated with BrdU

12   antibodies were added to the RNA samples. After 1 hour of incubation at room

13   temperature on a rotator the beads were washed four times in 1x BrU-IP buffer.

14   For elution of immunoprecipitated RNA the beads were resuspended in 200 µl

15   0.1% SDS. RNA was purified by phenol/chloroform extraction, ethanol

16   precipitation and the RNA pellets were resuspended in 10 µl nuclease free

17   water. 2 µl of immunoprecipitated RNA was used for quantification of mRNA

18   expression levels by RT-qPCR as described in the section 'Quantitative PCR'

19   except that DNase treatment was omitted and 1 µg yeast RNA (Roche, Basel,

20   Switzerland) was added in the cDNA reaction.

21

22   *BrU-labeling and immunoprecipitation of newly synthesized RNA*

23   The BrU-labeling and immunoprecipitation of newly labeled RNA were carried

24   out as for the mRNA decay assay except that the cells were harvested 45 min

25   after addition of BrU to the cell culture medium. Furthermore, after binding of

1   the RNA to the beads, the beads were washed once in 1x BrU-IP buffer, twice

2   in 1x BrU-IP buffer supplemented with 0.01% Triton X-100 and twice in 1x BrU-

3   IP buffer.

4

5   *Subcellular fractionation of nuclear and cytoplasmic RNA*

6   Subcellular fractionation of nuclear and cytoplasmic RNA was carried out as

7   previously described(Hollensen et al., 2018). Briefly, cells were washed in PBS,

8   then 800 μl PBS was added and the cells were scraped off. 100 µl of the cell

9   solution was centrifuged at 12,000 rpm for 10 sec at 4°C. Cell pellets were used

10   for purification of total RNA using 1 ml of TRI Reagent (Sigma-Aldrich)

11   according to manufacturer's protocol. The remaining 700 µl of the cell solution

12   was used for subcellular fractionation of nuclear and cytoplasmic RNA. After

13   centrifugation at 12,000 rpm for 10 sec at 4°C 300 µl lysis buffer (20 mM Tris-

14   HCl (pH 7.5), 140 mM NaCl, 1 mM EDTA, 0.5% Igepal-630 (Nonidet P-40))

15   were added to the cell pellets, which were then incubated on ice for 2 min and

16   centrifugated at 1,000 g for 4 min at 4°C. Cytoplasmic RNA was purified from

17   the supernatants using 1 ml TRI Reagent (Sigma-Aldrich) according to the

18   manufacturer's protocol. Pellets were washed twice in 500 µl lysis buffer,

19   subjected to a single 5 sec pulse of sonication at the lowest settings (Branson

20   Sonifier 250) and nuclear RNA was purified using 1 ml TRI Reagent (Sigma-

21   Aldrich) according to the manufacturer's protocol.

22

23   *Subcellular fractionation of nuclear and cytoplasmic protein*

24   Cells were washed in PBS, then 800 μl PBS were added and the cells were

25   scraped off. 80 µl of the cell solution was centrifuged at 500 g for 5 min and 200

1   µl lysis buffer (1x TBS, 0.5% Igepal-630 (Nonidet P-40)) were added to the cell

2   pellets for isolation of total protein. The remaining 720 µl of the cell solution was

3   used for subcellular fractionation of nuclear and cytoplasmic protein. After

4   centrifugation at 12,000 rpm for 10 sec at 4°C cell 300 µl lysis buffer were added

5   and the cell pellets, which were incubated on ice for 2 min and centrifugated at

6   1,000 g for 4 min at 4°C. The supernatants (cytoplasmic fractions) were

7   transferred to new tubes. Pellets (nuclear fractions) were washed twice in 500

8   µl lysis buffer and once in 500 µl 1x TBS and resuspended in 200 µl lysis buffer.

9   All samples were subjected to two 5 sec pulses of sonication at the lowest

10   settings (Branson Sonifier 250) followed by centrifugation at 4,000 g for 25 min

11   at 4°C. Supernatants were transferred to new tubes containing 87% glycerol

12   (final concentration of 10%) and concentrations were adjusted using Bio-Rad

13   protein assay (Bio-Rad, Hercules, California, United States).

14

15   *Quantitative PCR*

16   RNA was purified using TRI reagent (Thermo Scientific) according the to

17   manufacturer's protocol. RNA samples were treated with DNase I (Thermo

18   Scientific) according to the manufacturer's protocol. First-strand cDNA

19   synthesis was carried out using the Maxima First Strand cDNA synthesis Kit for

20   qPCR (Thermo Scientific) according to the manufacturer's protocol. qPCR

21   reactions were prepared using gene-specific primers (Table S4) and Platinum

22   SYBR Green qPCR Supermix-UDG (Thermo Scientific) according to the

23   manufacturer's protocol. An AriaMx Real-time PCR System (Agilent

24   Technologies) was used for quantification of RNA levels and the X_0 method

25   was used for calculations of relative RNA levels (Thomsen, Solvsten, Linnet,

1   Blechingberg, & Nielsen, 2010) normalized to either GAPDH or beta-actin

2   mRNA as indicated.

3

4   *NanoString*

5   Gene expression analysis of 770 neuropathology-related genes were analyzed

6   using the nCounter Human Neuropathology Panel (NanoString Technologies,

7   Seattle, Washington, United States) and the nCounter *SPRINT* Profiler

8   (NanoString Technologies) according to manufacturer's protocol. Data

9   analysis was carried out in the nSolver 4.0 software (NanoString Technologies)

10   using the nCounter Advanced Analysis Software (NanoString Technologies).

11

12   *Cell cycle assay*

13   Lentiviral transduction and RA-mediated differentiation of L-AN-5 cells were

14   carried out as described in the section 'circRNA knockdown and differentiation

15   of L-AN-5 cells'. Labeling of newly synthesized DNA was carried out using

16   Click-iT Plus EdU Alexa Flour 647 Flow Cytometry Assay Kit (Thermo

17   Scientific) according to manufacturer's protocol. Notably, the cell culture

18   medium of L-AN-5 cells cultured in 6-well plates was supplemented with 10 µM

19   EdU for 1.5 hours. To stain total DNA, cells with already detected EdU were

20   resuspended in 400 µl 1x Click-iT saponin-based permeabilization and wash

21   reagent from the Click-iT Plus EdU Alexa Flour 647 Flow Cytometry Assay Kit

22   (Thermo Scientific). Subsequently, RNase A was added to a final concentration

23   of 0.2 mg/ml. After 5 min of incubation at room temperature, propidium iodide

24   was added to a final concentration of 5 µg/ml and the cells were incubated for

25   30 min at room temperature. Incorporated EdU and total DNA levels were

1   analyzed on a BD LSRFortessa flow cytometer (BD Biosciences). Data analysis

2   was carried out in the FLOWJO software (BD Biosciences). The gating strategy

3   is shown in Figure S2F.

4

5   *Western blotting*

6   Cells were scraped off, pelleted and lysed for 15 min on ice in RSB100 (10 mM

7   Tris-HCl (pH 7.4), 100 mM NaCl, 2.5 mM $MgCl_2$) supplemented with 0.5%

8   Triton X-100 and 1 pill Complete® protease inhibitor cocktail (Roche). The cell

9   lysates were subjected to two 5 sec pulses of sonication at the lowest settings

10 (Branson Sonifier 250) followed by centrifugation at 4,000 g for 15 min at 4°C.

11 Glycerol was added to the supernatants (final concentration: 10%) and protein

12 concentrations were adjusted using Bio-Rad protein assay (Bio-Rad). The

13 protein samples were diluted in 6x loading buffer (9.8% glycerol, 12% SDS, 375

14 mM Tris-HCl (pH 6.8), 0.03% bromophenol blue, 10% β-mercaptoethanol),

15 heated at 95°C for 3 min and seprated on a Novex WedgeWell 4-12% Tris-

16 Glycine Gel (Invitrogen). Proteins were transferred to an PVDF Transfer

17 Membrane (Thermo Scientific) using standard procedures. The membranes

18 were blocked in 5% skimmed milk powder in PBS for 1 hour at room

19 temperature. The membranes were incubated at 4°C overnight with primary

20 antibodies diluted as indicated in Table S5 in 5% skimmed milk powder in PBS.

21 After three times wash, the membranes were incubated with goat polyclonal

22 HRP-conjungated secondary antibodies (Dako, Glostrup, Denmark) diluted

23 1:20,000 in 5% skimmed milk powder in PBS. After 1 hour of incubation at room

24 temperature, the membranes were washed three times and the bound

25 antibodies were detected using the SuperSignal West Femto maximum

1   sensitivity substrate (Thermo Scientific) according to the manufacturer's

2   protocol and using the LI-COR Odyssey system (LI-COR Biosciences, Lincoln,

3   Nebraska, United States).

4

5   *In vitro transcription*

6   As DNA templates for *in vitro* transcription, pcDNA3/circRNA vectors encoding

7   the full-length exonic sequences of five human circRNAs were used.

8   Biotinylated RNAs were produced from 0.5 µg linearized, and

9   phenol/chloroform extracted template using the MEGAscript® T7 Transcription

10   Kit (Ambion, Austin, Texas, United States), according to the manufacturer's

11   protocol with addition of 0.75 mM Biotin-14-CTP (Invitrogen) to the transcription

12   reaction. In controls, nuclease free water was added instead of Biotin-14-CTP.

13   The transcribed RNA was purified by phenol/chloroform extraction and

14   dissolved in nuclease free water.

15

16   *Streptavidin-Biotin pull-down*

17   For each pull-down, 125 µL (bead volume) Pierce® Streptavidin magnetic

18   beads (Thermo Scientific) pre-washed in NET-2 buffer (50 mM Tris-HCl pH 7.5,

19   150 mM NaCl, 0.1% Triton X-100) were incubated with 30 µg *in vitro*

20   synthesized circRNAs or 30 µg control RNA in 500 µL NET-2 buffer for 1 hr.

21   4°C mixing end-over-end. The conjugated beads were washed once in NET-2

22   buffer and incubated with 1.5 mL cell lysate prepared as follows: For each pull

23   down, one 90% confluent 150 mm plate of differentiated L-AN-5 cells was

24   washed in 10 mL ice cold PBS, and subjected to cell lysis in 1.5 mL hypotonic

25   gentle lysis buffer (10 mM Tris-HCl pH 7.5, 10 mM NaCl, 2 mM EDTA pH 8.0,

1   0.1% Triton X-100) supplemented with Complete® protease inhibitor cocktail

2   (Roche, 1 pastel per 10 mL lysis buffer) for 5 min. on ice. Cells were collected

3   by scraping and re-suspension, then supplemented with NaCl to 150 mM final

4   concentration and incubated on ice for 5 min. Cleared cell lysate was obtained

5   by centrifugation at 14,000 rpm, 4°C, 10 min. and supplemented with 10 µL

6   Ribolock RNase Inhibitor (40 U/µL, Thermo Scientific) per 10 mL lysis before

7   incubation with circRNA-coupled streptavidin beads for 1.5 hrs., 4°C mixing

8   end-over-end. From the cleared lysate 1% was mixed 1:1 with 2xSDS-load

9   buffer (20% glycerol, 4% SDS, 100 mM Tris-HCL pH 6.8, 0.05% Bromophenol

10   blue/Xylene cyanol and 10% β-mercaptoethanol) and kept as input sample.

11   Following capture of proteins, beads were washed four times in NET-2 buffer

12   and bound proteins were eluted in 40 µL preheated 2x SDS-load buffer by

13   boiling at 90°C for 5 min. Eluates were subjected to SDS-PAGE electrophoresis

14   and run either completely through and stained with SilverQuest™ Silver staining

15   kit (Life Technologies, Carlsbad, California, United States) according to the

16   manufacturer's protocol, or only 1.5 cm into the gel for subsequent staining with

17   GelCode® Blue Stain Reagent (Thermo Scientific) according to the

18   manufacturer's protocol and excision of the bands for mass spectrometry

19   application (see below).

20

21   *Protein analysis by nano-LC-MS/MS*

22   Interacting proteins were identified and quantified according to previously

23   described methods(Britze, Birkler, Gregersen, Ovesen, & Palmfeldt, 2014).

24   Briefly, each gel lane was cut into 1×1 mm pieces and cysteine residues were

25   blocked by reduction and alkylation using tris(2-carboxyethyl)phosphine and

1   iodoacetamide, respectively. In-gel digestion was performed using trypsin and

2   resulting peptides were extracted from gel pieces using acetonitrile and

3   trifluoroacetic acid and finally purified on PepClean C-18 Spin columns (Thermo

4   Scientific). Liquid chromatography tandem mass spectrometry (LC-MS/MS)

5   was performed on an EASY nanoLC coupled to a Q Exactive Plus Hybrid

6   Quadrupole-Orbitrap Mass Spectrometer (Thermo Scientific). Peptide samples

7   were separated on a C-18 reverse phase column (EASY-Spray PepMap from

8   Thermo Scientific with 25 cm length, 75 µm inner diameter, and 2 µm particle

9   size) and eluted by a 90 minutes linear gradient of acetonitrile (4–40%)

10   containing 0.1% formic acid. The MS was operated in data dependent mode,

11   automatically switching between MS and MS2 acquisition, with mass resolution

12   of 70,000 and 17,500, respectively. Up to 10 most intense ions were

13   fragmented per every full MS scan, by higher-energy collisional dissociation.

14   Dynamic exclusion of 10 seconds was applied and ions with single charge or

15   unassigned charge states were excluded from fragmentation.

16   MaxQuant software version 1.5.2.8 was applied for protein identification and

17   label-free quantification by means of peptide peak areas (Cox & Mann, 2008).

18   MS raw files were searched against a database consisting of 20,197 *Homo*

19   *sapiens* sequences downloaded from Uniprot.org, August 2015.

20   Carbamidomethylation of cysteines was set as a fixed modification whereas

21   methionine oxidation and protein N-terminal acetylation were set as dynamic

22   modifications. The false discovery rate (FDR) was assessed by searching

23   against a reverse decoy database, and FDR thresholds of protein and peptide

24   identification were both set to 0.01.

25

1   *Immunofluorescence*

2   For indirect immunofluorescence experiments, 1 x 10⁵ HEK293 Flp-In T-Rex or

3   circZNF827_HEK293 Flp-In T-Rex cells were grown directly on poly-L-lysine

4   coated coverslips in 12-well plates. Transcription of circRNA transgene was

5   induced by addition of 10-250 ng/ml tetracycline and the induction profile was

6   tested by Northern blotting in a parallel experiment. 24 hrs later cells were fixed

7   in 4% paraformaldehyde for 15 min, and permeabilized and blocked with

8   PBS/1% goat serum (or horse serum)/0.5% Triton X-100 for 20 min. Cells were

9   then incubated for 1-16 hrs with mouse anti-hnRNPK (Abcam, Cambridge,

10 United Kingdom), Rabbit anti-hnRNPU (Santa Cruz Biotechnologies, Dallas,

11 Texas, United States) or mouse anti-hnRNPL (Abcam). Antibodies were used

12 at 1:1,000 dilutions. Following removal of the primary antibody, cells were

13 incubated for 1 h with 4 µg/mL secondary anti-IgG antibodies labeled with

14 Alexa-594 and Alexa-488 (Molecular Probes, Eugene, Oregon, United States).

15

16 *RNA immunoprecipitation and co-immunoprecipitation of proteins*

17 For RNA immunoprecipitation (IP) and co-immunoprecipitation (co-IP) of

18 proteins L-AN-5 cells were seeded at a density of 6.6 x 10⁶ cells/dish in 10-cm

19 dishes and differentiated as described in the section 'Cell culturing'. HEK293

20 Flp-In T-Rex cells were seeded a density of 6.6 x 10⁶ cells/dish in 10-cm dishes.

21 HEK293 Flp-In T-Rex and HEK293 Flp-In T-Rex circZNF827 cells were

22 transfected with 5 µg pcDNA5/FRT-TO-FLAG-RBP and 25 µl polyethylenimine

23 (PEI) (1 µg/µl) according to a standard PEI transfection protocol. 6 hrs after

24 transfection, RBP and circRNA expression were induced by addition of 100

25 ng/ml tetracycline to the cell culture medium. For IP of endogenously expressed

1   proteins, antibodies were conjugated to Protein G dynabeads (Thermo

2   Scientific) prior to harvest of the cells. 25 μl beads per sample were washed

3   three times in 1 ml NET-2 buffer (50 mM Tris-HCl pH 7.5, 100 mM NaCl, 0.1%

4   Triton-X100). Subsequently, the beads were resuspended in 800 μl NET-2

5   buffer per sample and added 10 μl hnRNP K, hnRNP L, or IgG antibody per

6   sample. After conjugation for 120 min at 4°C on a rotator, the beads were

7   washed twice in NET-2 buffer and resuspended in 50 μl NET-2 buffer per

8   sample. For IP of FLAG-tagged proteins, 50 μl anti-FLAG-M2 agarose slurry

9   was washed twice in 1.5 ml NET-2 buffer and resuspended in 50 μl NET-2

10   buffer per sample. The cells were lysed after a single wash in PBS by addition

11   of 1 ml ice-cold hypotonic gentle lysis buffer (10 mM Tris-HCl pH 7.5, 10 mM

12   NaCl, 1 mM EDTA, 0.25% Triton-X100, and one pill Complete® protease

13   inhibitor cocktail (Roche) per 10 ml), scraped off, and transferred to an

14   Eppendorf tube. After incubation for 5 min on ice 35 μl 4 M NaCl (final 150 mM)

15   was added and the samples were incubated for 2 min on ice. The lysates were

16   subjected to a single 5 sec pulse of sonication at the lowest settings (Branson

17   Sonifier 250) and centrifuged at 13,000 rpm for 15 min at 4°C. For input protein

18   and RNA controls, 50 μl and 100 μl of the lysate were resuspended in 50 μl

19   2xSDS-load buffer (20% glycerol, 4% SDS, 100 mM Tris-HCL pH 6.8, 0.05%

20   Bromophenol blue/Xylene cyanol and 10% β-mercaptoethanol) and 1 ml TRI

21   Reagent (Sigma-Aldrich), respectively. The input protein control samples were

22   incubated for 3 min at 80-90˚C before storage at -20˚C. The remainder of the

23   supernatants was transferred to tubes containing 50 μl bead slurry and nutated

24   at 4˚C for 2 h. Subsequently, the beads were washed seven times in 1.5 ml ice-

25   cold NET-2 and protein was eluted form one third of the beads by addition of

1   100 μl 2xSDS-load buffer followed by incubation for 3 min at 80-90˚C whereas

2   RNA was eluted from two thirds of the beads by addition of 1 ml TRI Reagent

3   (Sigma-Aldrich).

4

5   *Northern blotting*

6   Northern blots were carried out as previously described in(Damgaard & Lykke-

7   Andersen, 2011). Briefly, 10 μg RNA was separated on a 1.2% formaldehyde-

8   agarose gel. Subsequently, the RNA was transferred to a Hybond membrane

9   (GE Healthcare, Chicago, Illinoise, United States). The membrane was

10   hybridized with circZNF827- or β-actin-specific [^{32}P]-end-labeled

11   oligonucleotides (sequences are specified in Table S4) overnight and

12   subsequently exposed on phosphorimager screens and visualized on a

13   Typhoon FLA 9500 (GE Healthcare).

14

15   *ChIP*

16   Lentiviral transduction and RA-mediated differentiation of L-AN-5 cells were

17   carried out as described in the section 'circRNA knockdown and differentiation

18   of L-AN-5 cells'. The ChIP assay including crosslinking and harvest of cells

19   were carried out using the Pierce Magnetic ChIP Kit (Thermo Scientific)

20   according to the manufacturer's protocol except that sonication was carried out

21   on a Covaris S2 ultrasonicator (settings: burst: 15%, cycles: 200, intensity: 6,

22   cycle time: 20 min, frequency sweeping: on, de-gas: on). The antibodies used

23   for the ChIP assay are listed in Table S5. DNA fragments were quantified as

24   described in the section 'Quantitative PCR' using the gene-specific primers

25   listed in Table S4.

43

1

2 *Statistical Analysis*

3 In biochemical assays (conducted in at least biological triplicates) the

4 significance of difference between samples were calculated by a two-tailed

5 Student's t test to test the null hypothesis of no difference between the two

6 compared groups. The assumption of equal variances was tested by an F test.

7 $p < 0.05$ was considered statistically significant. Data are presented as mean $\pm$

8 SD.

9

10 **Acknowledgements**

11 Proliferation assays using flow cytometry was performed at the FACS Core

12 Facility, Aarhus University, Denmark. Karina Hjorth is thanked for excellent

13 technical assistance. Thanks to Serafin Pinol-Roma for sharing anti-hnRNP

14 C1/C2 antibody.

15

16 **Competing interests**

17 The authors declare no competing interests.

18

19

20 **Figure Legends**

21

22 **Figure 1 - Determining the circRNA inventories of mESC, NPC and**

23 **differentiated glutamatergic neurons and their differential regulation.**

24 (A) Schematic illustration of workflow for differentiation and RNA-seq. (B)

25 Number of circRNAs detected by indicated circRNA prediction algorithm in

1   different stages. (C) Venn-diagram showing 1449 common circRNAs of a total

2   of 3581 circRNAs predicted by the different algorithms (as indicated next to the

3   diagram) that are either constant or enriched upon RNase R treatment. (D)

4   circRNA/circRNA+linear precursor ratios as a function of expression level

5   (RPM) at the 3 sequenced stages. (E) Left: Heatmap showing differential

6   expression of top-100 expressed circRNAs (RPM scale to the right), with

7   selected examples of circRNAs as indicated along with genomic coordinates

8   (mm10). Top: K-means analysis displaying 5 different expression profiles

9   during differentiation (same color code given to the left of the heatmap). (F)

10   circRNA qRT-PCR strategy spanning the backsplicing junction. (G) qRT-PCR

11   validaton of selected circRNAs. Data are depicted as mean ±SD.

12

13   **Figure 2 - circZNF827 regulates neuronal marker expression levels.**

14   (A) RT-qPCR analysis evaluating knockdown of circZNF827 with dicer-

15   independent short hairpin RNAs (dishRNAs) in the neuroblastoma cell line L-

16   AN-5. (B) Relative mRNA levels of the neuronal markers *TUBB3*, *MAP2*, *NEFL*,

17   and *TrkB* evaluated by RT-qPCR upon knockdown of circZNF827. The mRNA

18   expression levels were evaluated by RT-qPCR after four days of RA-mediated

19   neuronal differentiation. (C) Western blotting (left panel) of TUBB3 and MAP2

20   upon circZNF827 knockdown. GAPDH was used as loading control. The results

21   of quantification of band intensities from Western blots are shown in middle and

22   right panel. (D) Cell cycle assay based on flow cytometric measurements of

23   EdU incorporation into newly synthesized DNA in L-AN-5 cells upon

24   circZNF827 knockdown. +RA: differentiated L-AN-5 cells. -RA: undifferentiated

25   L-AN-5 cells. Irr: Irrelevant dishRNA. In all panels data are depicted as mean

1   ±SD. Asterisks above bars indicate statistical significance difference relative to

2   the control (Irr). *p<0.05; **p<0.01; ns, not significant.

3

4   **Figure 3 - Increased *RAR* expression upon circZNF827 knockdown.**

5   (A) mRNA expression levels of the RAR receptors *RARα*, *RARβ* and *RARγ* in

6   L-AN-5 cells upon circZNF827 knockdown evaluated by RT-qPCR. (B)

7   Subcellular localization of the circRNAs circZNF827, circANKIB1, and

8   circTULP4 examined by RT-qPCR after fractionation of differentiated L-AN-5

9   cells into cytoplasmic and nuclear fractions. *GAPDH* mRNA and β-actin pre-

10   mRNA levels was used for validation of the purity of the cytoplasmic and

11   nuclear fractions. (C) BrU pulse-chase mRNA decay assay evaluating decay

12   rates of *RAR* mRNAs upon circZNF827 knockdown. The *RAR* mRNA

13   expression levels were evaluated by RT-qPCR. In right panel, half-lives of the

14   *RARs* obtained in the experiment are indicated. +RA: differentiated L-AN-5

15   cells. -RA: undifferentiated L-AN-5 cells. Irr: Irrelevant dishRNA. In all panels

16   data are depicted as mean ±SD. Asterisks above bars indicate statistical

17   significance difference relative to the control (Irr). *p<0.05; **p<0.01.

18

19   **Figure 4 - circZNF827 regulates NGFR expression.**

20   (A) Volcano plot based on a Nanostring analysis of the expression of ~800

21   neuropathology-related genes upon circZNF827 knockdown in L-AN-5 cells vs

22   control without RA treatment (left panel) or with RA treatment (right panel). (B)

23   GO-term analysis based on genes found differentially expressed by the

24   Nanostring analysis upon circZNF827 knockdown in differentiated L-AN-5 cells.

25   (C) Western blotting (left panel) of NGFR upon circZNF827 knockdown in L-

1   AN-5 cells. GAPDH was used as loading control. The result of quantification of

2   band intensities from the Western blots is shown in the right panel. (D) BrU

3   pulse-chase mRNA decay assay evaluating decay rates of *NGFR* mRNAs upon

4   circZNF827 knockdown. In the bottom panel, the half-lives of NGFR obtained

5   in the experiment are indicated. (E) Volcano plot showing mRNAs with changed

6   synthesis rates estimated after BrU-labeling of newly synthesized RNA by

7   Nanostring analysis using the neuropathology panel. (F) RT-qPCR-based

8   validation of the Nanostring analysis shown in (E). (G) Evaluation of

9   circZNF827 knockdown in L-AN-5 cells after subcellular fractionation into

10   nuclear and cytoplasmic RNA fractions by RT-qPCR. *GAPDH* mRNA and *β-*

11   *actin* pre-mRNA levels was used for validation of the purity of the cytoplasmic

12   and nuclear fractions. (H) *c-fos* mRNA levels evaluated by RT-qPCR after

13   circZNF827 knockdown and NGF stimulation of L-AN-5 cells. +RA:

14   differentiated L-AN-5 cells. -RA: undifferentiated L-AN-5 cells. Irr: Irrelevant

15   dishRNA. Data are depicted in C as mean ±SEM and in D, F, and G as mean

16   ±SD. Asterisks above bars indicate statistical significance difference relative to

17   the control (Ir10r). *p<0.05, **p<0.01, ***p<0.001.

18

19   **Figure 5 – circZNF827 interacts with and regulates the subcellular**

20   **localization of hnRNP K and -L.**

21   (A) circRNA-RBP complex isolation from differentiated L-AN-5 cells followed by

22   protein identification using mass spectrometry (LC-MS/MS). IP/Input ratios

23   (based on IBAQ values) for selected RBPs (hnRNP L, hnRNP L, hnRNP U,

24   DDX3X and DHX9) pulled down by circZNF827 are shown in left panel. In the

25   right panel IP ratios of selected RBPs pulled down by circZNF827 relative to IP

1   ratios for four other circRNAs (circTULP4, circHDGFRP3, circSLC8A1 and

2   circZNF609) are shown. RIP experiment evaluating interaction between

3   circZNF827 and hnRNP K and -L in differentiated L-AN-5 cells (B) and the

4   HEK293 Flp-In T-rex circZNF827 cell line (C). Co-immunoprecipitation (co-IP)

5   of both exogenously FLAG-tagged (D) and endogenously (E) expressed

6   hnRNP K, -L and -U in HEK293 Flp-In T-rex cells with and without circZNF827

7   expression. GAPDH and HuR were used as loading controls in (D) and (E)

8   respectively. (F) Western blot evaluating subcellular localization of hnRNP K

9   in differentiated L-AN-5 cells upon circZNF827 knockdown. LARP1 and hnRNP

10   C1/C2 were used for validation of the purity of the cytoplasmic and nuclear

11   fractions. (G) Co-immunofluorescence (co-IF) of hnRNP K, -L and -U in

12   HEK293 Flp-In T-rex cells upon circZNF827 overexpression. Nuclei were

13   visualized by DAPI staining. The scale bar indicates 10 μm. Irr: Irrelevant

14   dishRNA. C: cytoplasmic fraction, N: nuclear fraction, T: total cell lysate.

15

16   **Figure 6 – circZNF827 regulates hnRNP K activity in L-AN-5 cells.** RT-

17   qPCR (A) and Western blotting (B) evaluating NGFR expression upon co-

18   knockdown of circZNF827 and either hnRNP K or -L in differentiated L-AN-5

19   cells. GAPDH was used as loading control for the Western blots. (C) ChIP

20   experiment assessing association between the NGFR gene and RNP PolII and

21   hnRNP K upon circZNF827 knockdown in differentiated L-AN-5 cells. (D) Co-

22   immunoprecipitation (co-IP) of ZNF827, hnRNP K and -L in cyto-/nucleoplasm

23   (left) or chromatin fractions (right; sonicated pellets from cleared lysates) of

24   differentiated L-AN-5 cells. IgG was used as IP control. HuR was used as

25   negative control. (E) RNA-immunoprecipitation of circZNF827 by ZNF827. IgG

1   was used as IP control. #1 and #2: two different dishRNAs targeting the same

2   RBP. Irr: Irrelevant dishRNA. Data in (A) are depicted as mean ±SD (three

3   biological replicates).

4

5   **Figure 7 – Model illustrating how circZNF827 could regulate transcription**

6   **from key neuronal genes**. The promoter of target genes, e.g. NGFR is bound

7   by a transcription repressive complex consisting of circZNF827, hnRNP K,

8   hnRNP L and ZNF827. High levels of circZNF827, induced by neuronal

9   differentiation keeps further differentiation markers in check (left panel), while

10   knockdown of circZNF827 (or hnRNP K/L) allows for higher transcription rates

11   of target neuronal marker genes including NGFR.

12

13   **Figure 1 – figure supplement 1** - (A) Brightfield image of mESCs subjected to

14   neuronal differention (neuron day 1, 3 and 8). (B) qRT-PCR on pluripotency

15   and neuronal markers (Nanog, Nestin, TrkB and TUBB3) at different stages in

16   differentiation. (C) Quantification of RNase R resistant circRNAs. Fraction of

17   either depleted, unaffected or enriched of total number of circRNAs upon

18   RNase R treatment as a result of using indicated circRNA prediction algorithm.

19   The red numbers in each column indicate the percentage of depleted ones. (D)

20   Expression levels of depleted, unaffected or enriched circRNAs (RPM). (E)

21   Distribution of length (nucleotides) of circRNA-flanking introns and introns

22   found in host pre-mRNAs. (F) Frequency of inclusion of 5'proximal exons in

23   circRNAs.

24   **Figure 2 – figure supplement 1** - (A) Evaluation of dishRNA-mediated

25   knockdown efficiencies of circZNF827 in mESCs, P19 cells and SHSY-5Y cells

1   by RT-qPCR. (B) Evaluation of mRNA expression levels of the neuronal

2   markers *TUBB3*, *MAP2*, *NEFL*, and *TrkB* upon RA-mediated neuronal

3   differentiation of SHSY-5Y cells by RT-qPCR. (C) Knockdown efficiencies of

4   the circRNAs circSLC8A1, circHDGFRP3, circCDYL, circZNF609,

5   circCAMSAP1, circUNC79, circANKIB1, and circTULP4 in L-AN-5 cells

6   measured by RT-qPCR using circRNA-specific primers.

7

8   **Figure 2 – figure supplement 2** - (A) mRNA expression levels of the neuronal

9   markers *TUBB3*, *MAP2*, *TrkB*, and *NEFL* upon circRNA knockdown in L-AN-5

10   cells evaluated by RT-qPCR. (B) Validation of linear ZNF827 (linZNF827)

11   mRNA levels upon knockdown of circZNF827 in L-AN-5 cells.

12

13   **Figure 2 – figure supplement 3** - (A) Gating strategy for the cell cycle assay

14   shown in Figure 2D. (B) Flow cytometric analysis of the cell cycle assay also

15   shown in figure 2D. For all conditions three biological replicates are shown.

16   +RA: differentiated L-AN-5 cells. -RA: undifferentiated L-AN-5 cells. Irr:

17   Irrelevant dishRNA. Data are depicted as mean ±SD.

18

19   **Figure 3 – figure supplement 1** - (A) *RAR* mRNA transcription rates estimated

20   after BrU-labeling of newly synthesized RNA by RT-qPCR. Data are depicted

21   as mean ±SD. Asterisks above bars indicate statistical significance difference

22   relative to the control (Irr). *p<0.05.

23

1   **Figure 4 – figure supplement 1** - (A) RT-qPCR evaluating *NGFR* mRNA

2   expression upon circZNF827 knockdown in L-AN-5 cells and NGF stimulation.

3   Data are depicted as mean ±SD.

4

5   **Figure 5 – figure supplement 1** - (A) Silver stain of circRNA-pull down

6   samples analyzed by LC-MS/MS. The negative controls included are circRNA

7   templates transcribed without biotin-CTP (circTULP4 neg and circZNF827

8   neg). The CTC is a lincRNA with a known binding profile included as reference.

9   (B-C) Prediction of hnRNP K and -L binding sites in the most 3' part of the

10   circZNF827-encoding sequence by RBPmap. (D) MFold prediction of the

11   secondary structure of circZNF827 shown with the predicted hnRNP K and -L

12   binding sites. (E) Schematic drawing of the stable HEK293 Flp-In T-rex cell-line

13   for Laccase2 vector-based expression of circZNF827 from a tetracycline

14   inducible promoter (CMV tet-on). (F) Northern blot showing induction profile for

15   circZNF827 expression in the stable HEK293 Flp-In T-rex circZNF827 cell-line.

16   Notably, circZNF827 is shown to be RNase R resistant whereas the linear

17   loading control (*β-actin* mRNA) is RNase R sensitive. SS: splice site, BSJ: back

18   splice junction.

19

20   **Figure 6 – figure supplement 1** - circRNA (A), hnRNP K and -L (B) knockdown

21   validation associated with results shown in Figure 6A-B. (A) Quantification of

22   circZNF827 levels by RT-qPCR. Protein levels are evaluated by Western

23   blotting in (B). GAPDH was used as loading control for the Western blots. (D)

24   ChIP-seq data (ENCODE consortium) in K562 and HepG2 cells showing

25   interaction between hnRNP K and the NGFR promoter. Y-axis displays

1   enrichment (fold change (FC)) over control. #1 and #2: two different dishRNAs

2   targeting the same RBP.

3

4   **References**

5

6   Abdelmohsen, K., Panda, A. C., Munk, R., Grammatikakis, I., Dudekula, D. B.,

7   De, S., . . . Gorospe, M. (2017). Identification of HuR target circular RNAs

8   uncovers suppression of PABPN1 translation by CircPABPN1. *RNA*

9   *Biol, 14*(3), 361-369. doi:10.1080/15476286.2017.1279788

10   AbouHaidar, M. G., Venkataraman, S., Golshani, A., Liu, B., & Ahmad, T.

11   (2014). Novel coding, translation, and gene expression of a replicating

12   covalently closed circular RNA of 220 nt. *Proc Natl Acad Sci U S A,*

13   *111*(40), 14542-14547. doi:10.1073/pnas.1402814111

14   Ashwal-Fluss, R., Meyer, M., Pamudurti, N. R., Ivanov, A., Bartok, O., Hanan,

15   M., . . . Kadener, S. (2014). circRNA biogenesis competes with pre-

16   mRNA splicing. *Mol Cell, 56*(1), 55-66.

17   doi:10.1016/j.molcel.2014.08.019

18   Bibel, M., Richter, J., Lacroix, E., & Barde, Y. A. (2007). Generation of a defined

19   and uniform population of CNS progenitors and neurons from mouse

20   embryonic stem cells. *Nat Protoc, 2*(5), 1034-1043.

21   doi:10.1038/nprot.2007.147

22   Bothwell, M. (2016). Recent advances in understanding neurotrophin signaling.

23   *F1000Res, 5*. doi:10.12688/f1000research.8434.1

24   Britze, A., Birkler, R. I., Gregersen, N., Ovesen, T., & Palmfeldt, J. (2014).

25   Large-scale proteomics differentiates cholesteatoma from surrounding

1   tissues and identifies novel proteins related to the pathogenesis. *PLoS*

2   *One, 9*(8), e104103. doi:10.1371/journal.pone.0104103

3   Capel, B., Swain, A., Nicolis, S., Hacker, A., Walter, M., Koopman, P., . . .

4   Lovell-Badge, R. (1993). Circular transcripts of the testis-determining

5   gene Sry in adult mouse testis. *Cell, 73*(5), 1019-1030. Retrieved from

6   https://www.ncbi.nlm.nih.gov/pubmed/7684656

7   Chekulaeva, M., & Rajewsky, N. (2018). Roles of Long Noncoding RNAs and

8   Circular RNAs in Translation. *Cold Spring Harb Perspect Biol*.

9   doi:10.1101/cshperspect.a032680

10   Chen, C. Y., & Sarnow, P. (1995). Initiation of protein synthesis by the

11   eukaryotic translational apparatus on circular RNAs. *Science,*

12   *268*(5209), 415-417. Retrieved from

13   https://www.ncbi.nlm.nih.gov/pubmed/7536344

14   Cocquerelle, C., Mascrez, B., Hetuin, D., & Bailleul, B. (1993). Mis-splicing

15   yields circular RNA molecules. *FASEB J, 7*(1), 155-160. Retrieved from

16   http://www.ncbi.nlm.nih.gov/pubmed/7678559

17   Conn, S. J., Pillman, K. A., Toubia, J., Conn, V. M., Salmanidis, M., Phillips, C.

18   A., . . . Goodall, G. J. (2015). The RNA binding protein quaking regulates

19   formation of circRNAs. *Cell, 160*(6), 1125-1134.

20   doi:10.1016/j.cell.2015.02.014

21   Cox, J., & Mann, M. (2008). MaxQuant enables high peptide identification rates,

22   individualized p.p.b.-range mass accuracies and proteome-wide protein

23   quantification. *Nat Biotechnol, 26*(12), 1367-1372. doi:10.1038/nbt.1511

1   Damgaard, C. K., & Lykke-Andersen, J. (2011). Translational coregulation of

2   5'TOP mRNAs by TIA-1 and TIAR. *Genes Dev, 25*(19), 2057-2068.

3   doi:10.1101/gad.17355911

4   Deveson, I. W., Hardwick, S. A., Mercer, T. R., & Mattick, J. S. (2017). The

5   Dimensions, Dynamics, and Relevance of the Mammalian Noncoding

6   Transcriptome. *Trends Genet, 33*(7), 464-478.

7   doi:10.1016/j.tig.2017.04.004

8   Ebbesen, K. K., Hansen, T. B., & Kjems, J. (2016). Insights into circular RNA

9   biology. *RNA Biol*, 1-11. doi:10.1080/15476286.2016.1271524

10 Gao, Y., Zhang, J., & Zhao, F. (2018). Circular RNA identification based on

11   multiple seed matching. *Brief Bioinform, 19*(5), 803-810.

12   doi:10.1093/bib/bbx014

13 Glazar, P., Papavasileiou, P., & Rajewsky, N. (2014). circBase: a database for

14   circular RNAs. *RNA, 20*(11), 1666-1670. doi:10.1261/rna.043687.113

15 Gudas, L. J., & Wagner, J. A. (2011). Retinoids regulate stem cell

16   differentiation. *J Cell Physiol, 226*(2), 322-330. doi:10.1002/jcp.22417

17 Hansen, T. B. (2018). Improved circRNA Identification by Combining Prediction

18   Algorithms. *Front Cell Dev Biol, 6*, 20. doi:10.3389/fcell.2018.00020

19 Hansen, T. B., Jensen, T. I., Clausen, B. H., Bramsen, J. B., Finsen, B.,

20   Damgaard, C. K., & Kjems, J. (2013). Natural RNA circles function as

21   efficient microRNA sponges. *Nature, 495*(7441), 384-388.

22   doi:10.1038/nature11993

23 Hansen, T. B., Veno, M. T., Damgaard, C. K., & Kjems, J. (2016). Comparison

24   of circular RNA prediction tools. *Nucleic Acids Res, 44*(6), e58.

25   doi:10.1093/nar/gkv1458

Havugimana, P. C., Hart, G. T., Nepusz, T., Yang, H., Turinsky, A. L., Li, Z., . . . Emili, A. (2012). A census of human soluble protein complexes. *Cell, 150*(5), 1068-1081. doi:10.1016/j.cell.2012.08.011

Hollensen, A. K., Andersen, S., Hjorth, K., Bak, R. O., Hansen, T. B., Kjems, J., . . . Mikkelsen, J. G. (2018). Enhanced Tailored MicroRNA Sponge Activity of RNA Pol II-Transcribed TuD Hairpins Relative to Ectopically Expressed ciRS7-Derived circRNAs. *Mol Ther Nucleic Acids, 13*, 365-375. doi:10.1016/j.omtn.2018.09.009

Hollensen, A. K., Thomsen, R., Bak, R. O., Petersen, C. C., Ermegaard, E. R., Aagaard, L., . . . Mikkelsen, J. G. (2017). Improved microRNA suppression by WPRE-linked Tough Decoy microRNA sponges. *RNA*. doi:10.1261/rna.061192.117

Huang, C., Liang, D., Tatomer, D. C., & Wilusz, J. E. (2018). A length-dependent evolutionarily conserved pathway controls nuclear export of circular RNAs. *Genes Dev, 32*(9-10), 639-644. doi:10.1101/gad.314856.118

Huarte, M., Guttman, M., Feldser, D., Garber, M., Koziol, M. J., Kenzelmann-Broz, D., . . . Rinn, J. L. (2010). A large intergenic noncoding RNA induced by p53 mediates global gene repression in the p53 response. *Cell, 142*(3), 409-419. doi:10.1016/j.cell.2010.06.040

Hyun, D. H., Kim, J., Moon, C., Lim, C. J., de Cabo, R., & Mattson, M. P. (2012). The plasma membrane redox enzyme NQO1 sustains cellular energetics and protects human neuroblastoma cells against metabolic and proteotoxic stress. *Age (Dordr), 34*(2), 359-370. doi:10.1007/s11357-011-9245-1

1   Jeck, W. R., & Sharpless, N. E. (2014). Detecting and characterizing circular

2   RNAs. *Nat Biotechnol, 32*(5), 453-461. doi:10.1038/nbt.2890

3   Jeck, W. R., Sorrentino, J. A., Wang, K., Slevin, M. K., Burd, C. E., Liu, J., . . .

4   Sharpless, N. E. (2013). Circular RNAs are abundant, conserved, and

5   associated with ALU repeats. *RNA, 19*(2), 141-157.

6   doi:10.1261/rna.035667.112

7   Kaadt, E., Alsing, S., Cecchi, C. R., Damgaard, C. K., Corydon, T. J., &

8   Aagaard, L. (2019). Efficient Knockdown and Lack of Passenger Strand

9   Activity by Dicer-Independent shRNAs Expressed from Pol II-Driven

10   MicroRNA Scaffolds. *Mol Ther Nucleic Acids, 14*, 318-328.

11   doi:10.1016/j.omtn.2018.11.013

12   Kim, J. H., Hahm, B., Kim, Y. K., Choi, M., & Jang, S. K. (2000). Protein-protein

13   interaction among hnRNPs shuttling between nucleus and cytoplasm. *J

14   Mol Biol, 298*(3), 395-405. doi:10.1006/jmbi.2000.3687

15   Kleaveland, B., Shi, C. Y., Stefano, J., & Bartel, D. P. (2018). A Network of

16   Noncoding Regulatory RNAs Acts in the Mammalian Brain. *Cell, 174*(2),

17   350-362 e317. doi:10.1016/j.cell.2018.05.022

18   Kopp, F., & Mendell, J. T. (2018). Functional Classification and Experimental

19   Dissection of Long Noncoding RNAs. *Cell, 172*(3), 393-407.

20   doi:10.1016/j.cell.2018.01.011

21   Kos, A., Dijkema, R., Arnberg, A. C., van der Meide, P. H., & Schellekens, H.

22   (1986). The hepatitis delta (delta) virus possesses a circular RNA.

23   *Nature, 323*(6088), 558-560. doi:10.1038/323558a0

24   Kramer, M. C., Liang, D., Tatomer, D. C., Gold, B., March, Z. M., Cherry, S., &

25   Wilusz, J. E. (2015). Combinatorial control of Drosophila circular RNA

expression by intronic repeats, hnRNPs, and SR proteins. *Genes Dev, 29*(20), 2168-2182. doi:10.1101/gad.270421.115

Legnini, I., Di Timoteo, G., Rossi, F., Morlando, M., Briganti, F., Sthandier, O., . . . Bozzoni, I. (2017). Circ-ZNF609 Is a Circular RNA that Can Be Translated and Functions in Myogenesis. *Mol Cell, 66*(1), 22-37 e29. doi:10.1016/j.molcel.2017.02.017

Li, Z., Huang, C., Bao, C., Chen, L., Lin, M., Wang, X., . . . Shan, G. (2015). Exon-intron circular RNAs regulate transcription in the nucleus. *Nat Struct Mol Biol, 22*(3), 256-264. doi:10.1038/nsmb.2959

Lyu, J., Yu, X., He, L., Cheng, T., Zhou, J., Cheng, C., . . . Zhou, W. (2015). The protein phosphatase activity of PTEN is essential for regulating neural stem cell differentiation. *Mol Brain, 8*, 26. doi:10.1186/s13041-015-0114-1

Ma, X., Zhou, Y., Chai, Y., Wang, X., & Huang, X. (2017). Stat3 Controls Maturation and Terminal Differentiation in Mouse Hippocampal Neurons. *J Mol Neurosci, 61*(1), 88-95. doi:10.1007/s12031-016-0820-x

Memczak, S., Jens, M., Elefsinioti, A., Torti, F., Krueger, J., Rybak, A., . . . Rajewsky, N. (2013). Circular RNAs are a large class of animal RNAs with regulatory potency. *Nature, 495*(7441), 333-338. doi:10.1038/nature11928

Meola, N., Domanski, M., Karadoulama, E., Chen, Y., Gentil, C., Pultz, D., . . . Jensen, T. H. (2016). Identification of a Nuclear Exosome Decay Pathway for Processed Transcripts. *Mol Cell, 64*(3), 520-533. doi:10.1016/j.molcel.2016.09.025

Moumen, A., Masterson, P., O'Connor, M. J., & Jackson, S. P. (2005). hnRNP K: an HDM2 target and transcriptional coactivator of p53 in response to DNA damage. *Cell, 123*(6), 1065-1078. doi:10.1016/j.cell.2005.09.032

Nigro, J. M., Cho, K. R., Fearon, E. R., Kern, S. E., Ruppert, J. M., Oliner, J. D., . . . Vogelstein, B. (1991). Scrambled exons. *Cell, 64*(3), 607-613. Retrieved from https://www.ncbi.nlm.nih.gov/pubmed/1991322

Pamudurti, N. R., Bartok, O., Jens, M., Ashwal-Fluss, R., Stottmeister, C., Ruhe, L., . . . Kadener, S. (2017). Translation of CircRNAs. *Mol Cell, 66*(1), 9-21 e27. doi:10.1016/j.molcel.2017.02.021

Pasman, Z., Been, M. D., & Garcia-Blanco, M. A. (1996). Exon circularization in mammalian nuclear extracts. *RNA, 2*(6), 603-610. Retrieved from https://www.ncbi.nlm.nih.gov/pubmed/8718689

Paz, I., Kosti, I., Ares, M., Jr., Cline, M., & Mandel-Gutfreund, Y. (2014). RBPmap: a web server for mapping binding sites of RNA-binding proteins. *Nucleic Acids Res, 42*(Web Server issue), W361-367. doi:10.1093/nar/gku406

Piwecka, M., Glazar, P., Hernandez-Miranda, L. R., Memczak, S., Wolf, S. A., Rybak-Wolf, A., . . . Rajewsky, N. (2017). Loss of a mammalian circular RNA locus causes miRNA deregulation and affects brain function. *Science*. doi:10.1126/science.aam8526

Rybak-Wolf, A., Stottmeister, C., Glazar, P., Jens, M., Pino, N., Giusti, S., . . . Rajewsky, N. (2015). Circular RNAs in the Mammalian Brain Are Highly Abundant, Conserved, and Dynamically Expressed. *Mol Cell, 58*(5), 870-885. doi:10.1016/j.molcel.2015.03.027

Salzman, J. (2016). Circular RNA Expression: Its Potential Regulation and Function. *Trends Genet, 32*(5), 309-316. doi:10.1016/j.tig.2016.03.002

Salzman, J., Chen, R. E., Olsen, M. N., Wang, P. L., & Brown, P. O. (2013). Cell-type specific features of circular RNA expression. *PLoS Genet, 9*(9), e1003777. doi:10.1371/journal.pgen.1003777

Salzman, J., Gawad, C., Wang, P. L., Lacayo, N., & Brown, P. O. (2012). Circular RNAs are the predominant transcript isoform from hundreds of human genes in diverse cell types. *PLoS One, 7*(2), e30733. doi:10.1371/journal.pone.0030733

Sanger, H. L., Klotz, G., Riesner, D., Gross, H. J., & Kleinschmidt, A. K. (1976). Viroids are single-stranded covalently closed circular RNA molecules existing as highly base-paired rod-like structures. *Proc Natl Acad Sci U S A, 73*(11), 3852-3856. Retrieved from https://www.ncbi.nlm.nih.gov/pubmed/1069269

Seitz, A. K., Christensen, L. L., Christensen, E., Faarkrog, K., Ostenfeld, M. S., Hedegaard, J., . . . Dyrskjot, L. (2017). Profiling of long non-coding RNAs identifies LINC00958 and LINC01296 as candidate oncogenes in bladder cancer. *Sci Rep, 7*(1), 395. doi:10.1038/s41598-017-00327-0

Stagsted, L. V., Nielsen, K. M., Daugaard, I., & Hansen, T. B. (2019). Noncoding AUG circRNAs constitute an abundant and conserved subclass of circles. *Life Sci Alliance, 2*(3). doi:10.26508/lsa.201900398

Suenkel, C., Cavalli, D., Massalini, S., Calegari, F., & Rajewsky, N. (2020). A Highly Conserved Circular RNA Is Required to Keep Neural Cells in a Progenitor State in the Mammalian Brain. *Cell Rep, 30*(7), 2170-2179 e2175. doi:10.1016/j.celrep.2020.01.083

1   Thompson, P. J., Dulberg, V., Moon, K. M., Foster, L. J., Chen, C., Karimi, M.

2   M., & Lorincz, M. C. (2015). hnRNP K coordinates transcriptional

3   silencing by SETDB1 in embryonic stem cells. *PLoS Genet, 11*(1),

4   e1004933. doi:10.1371/journal.pgen.1004933

5   Thomsen, R., Solvsten, C. A., Linnet, T. E., Blechingberg, J., & Nielsen, A. L.

6   (2010). Analysis of qPCR data by converting exponentially related Ct

7   values into linearly related X0 values. *J Bioinform Comput Biol, 8*(5),

8   885-900. doi:10.1142/s0219720010004963

9   Tomonaga, T., & Levens, D. (1995). Heterogeneous nuclear ribonucleoprotein

10   K is a DNA-binding transactivator. *J Biol Chem, 270*(9), 4875-4881.

11   doi:10.1074/jbc.270.9.4875

12 Wan, C., Borgeson, B., Phanse, S., Tu, F., Drew, K., Clark, G., . . . Emili, A.

13   (2015). Panorama of ancient metazoan macromolecular complexes.

14   *Nature, 525*(7569), 339-344. doi:10.1038/nature14877

15 Yamashita, T., Tucker, K. L., & Barde, Y. A. (1999). Neurotrophin binding to the

16   p75 receptor modulates Rho activity and axonal outgrowth. *Neuron,*

17   *24*(3), 585-593. doi:10.1016/s0896-6273(00)81114-9

18 Yang, Y., Fan, X., Mao, M., Song, X., Wu, P., Zhang, Y., . . . Wang, Z. (2017).

19   Extensive translation of circular RNAs driven by N(6)-methyladenosine.

20   *Cell Res, 27*(5), 626-641. doi:10.1038/cr.2017.31

21 Ying, Q. L., Wray, J., Nichols, J., Batlle-Morera, L., Doble, B., Woodgett, J., . .

22   . Smith, A. (2008). The ground state of embryonic stem cell self-renewal.

23   *Nature, 453*(7194), 519-523. doi:10.1038/nature06968

24 Zhang, X. O., Dong, R., Zhang, Y., Zhang, J. L., Luo, Z., Zhang, J., . . . Yang,

25   L. (2016). Diverse alternative back-splicing and alternative splicing

1   landscape of circular RNAs. *Genome Res, 26*(9), 1277-1287.

2   doi:10.1101/gr.202895.115

3 Zhu, X., Libby, R. T., de Vries, W. N., Smith, R. S., Wright, D. L., Bronson, R.

4   T., . . . John, S. W. (2012). Mutations in a P-type ATPase gene cause

5   axonal   degeneration.   *PLoS   Genet, 8*(8),   e1002853.

6   doi:10.1371/journal.pgen.1002853

7

8

9

Figure 1
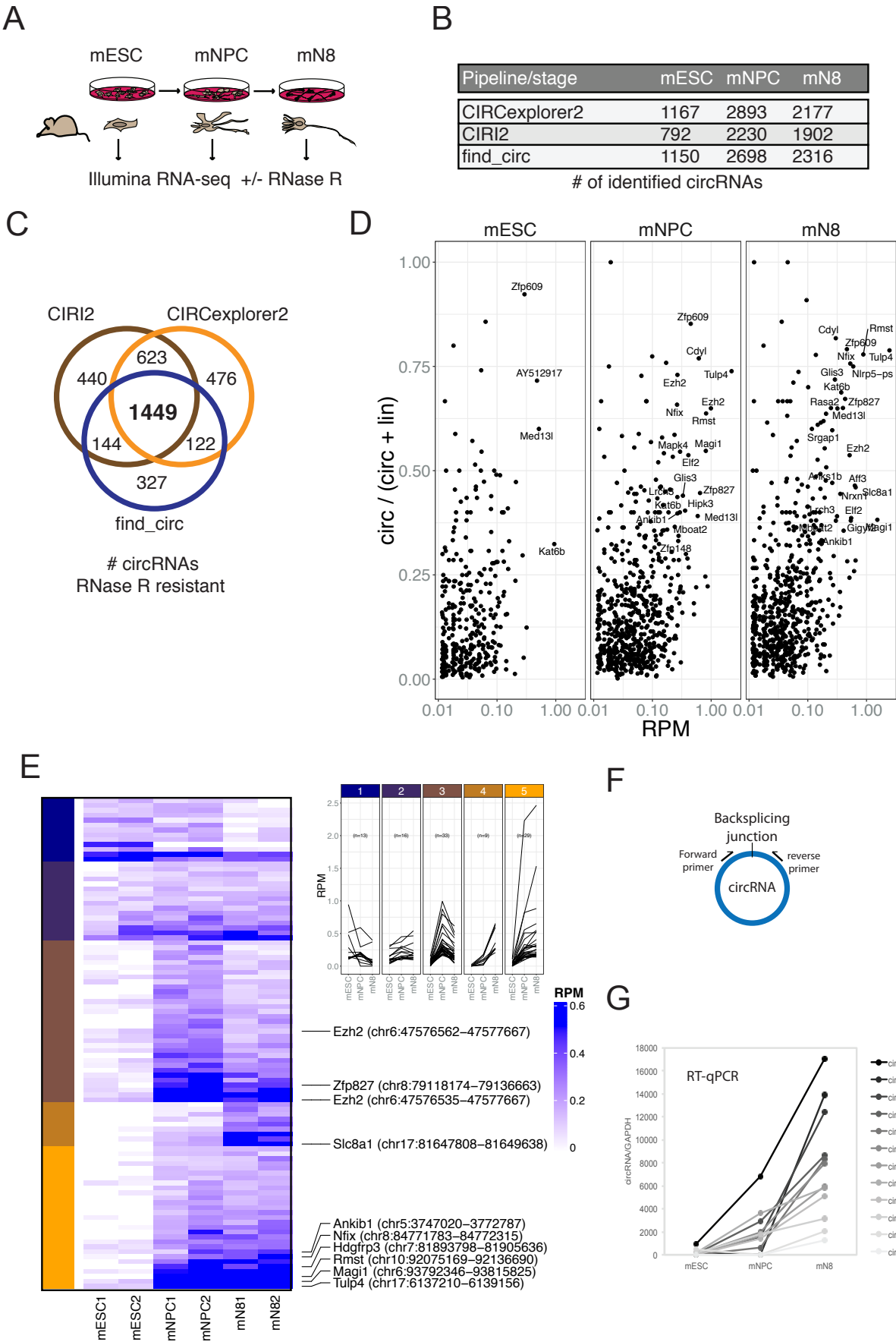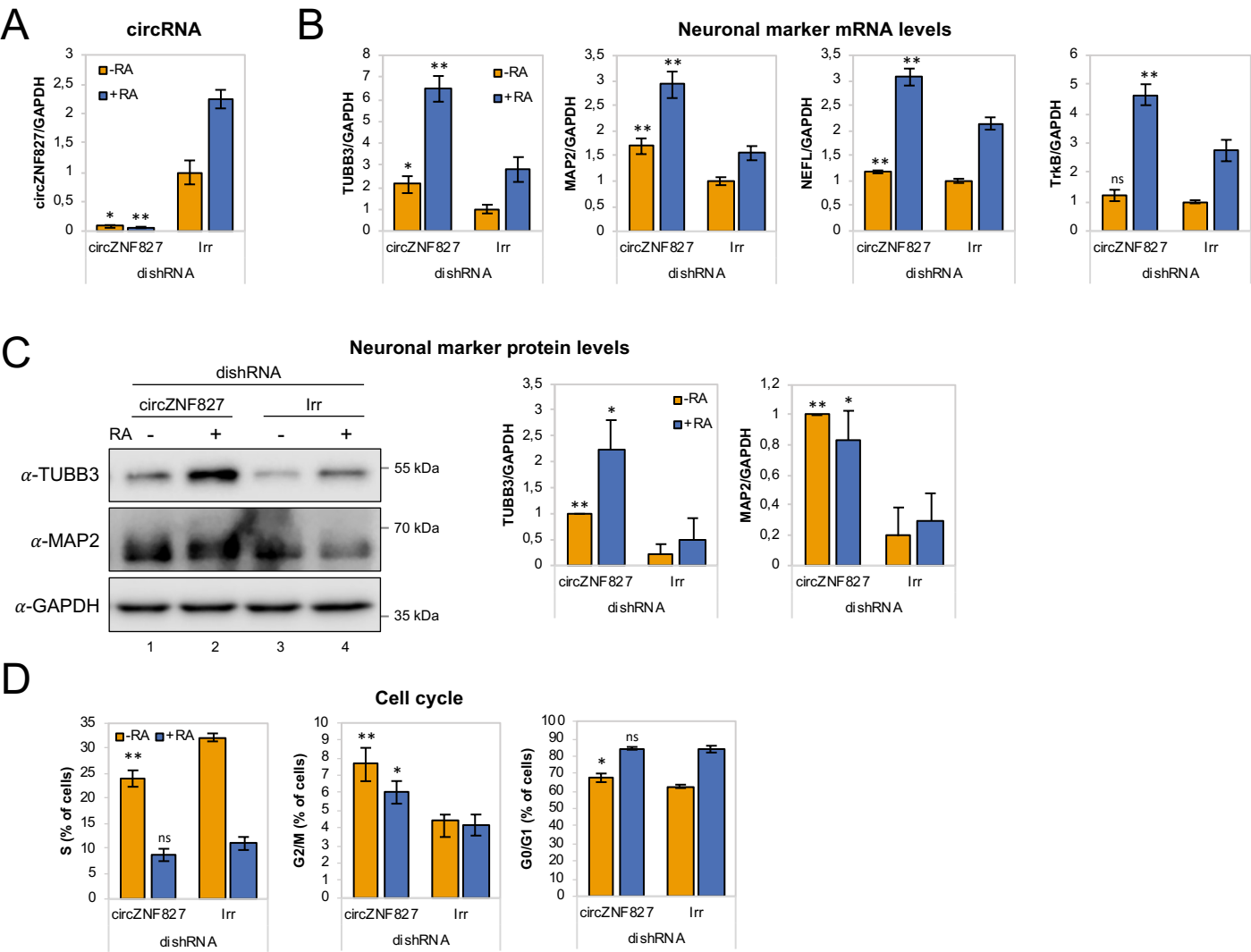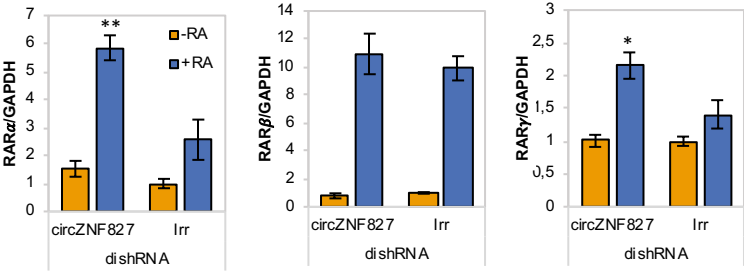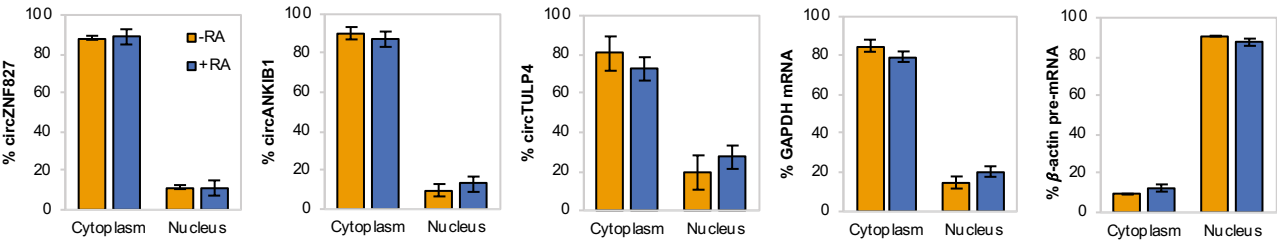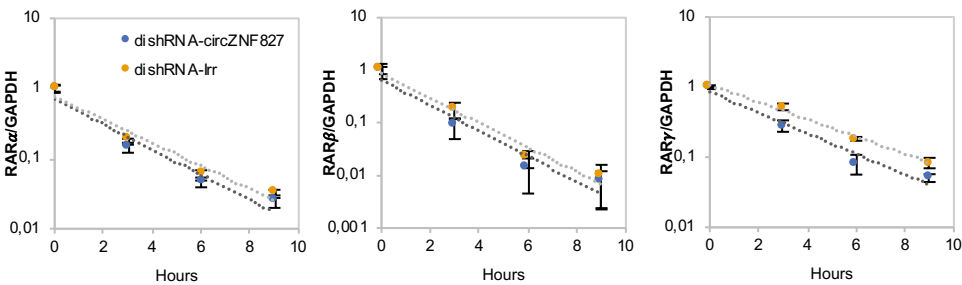
Hollensen et al., 2020

Figure 2

Hollensen et al., 2020

Figure 3

Figure 4

Hollensen et al., 2020

Figure 5

Figure 6

A

B

C

D

Differentiated L-AN-5
(cyto-/nucleoplasm)

Differentiated L-AN-5
(chromatin)

E

ZNF827 RIP
differentiated L-AN-5

Hollensen et al., 2020
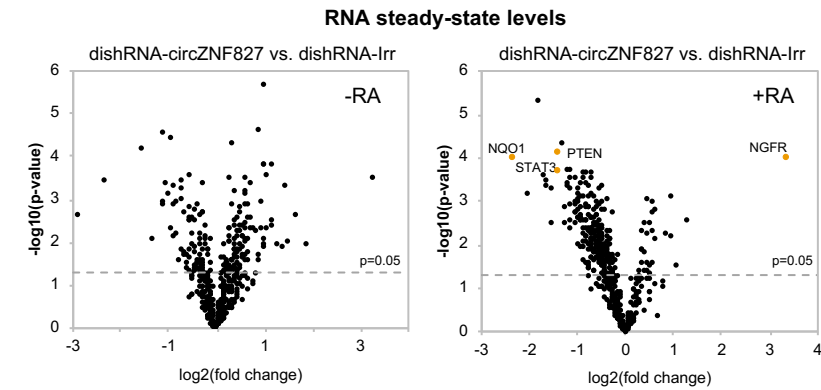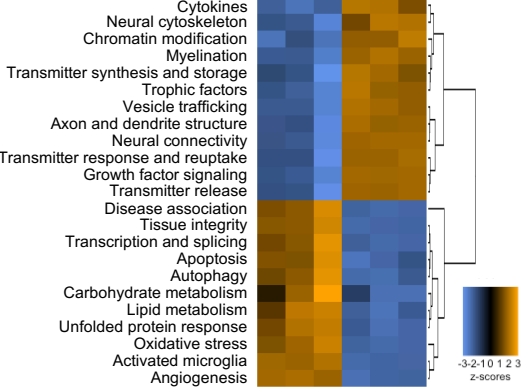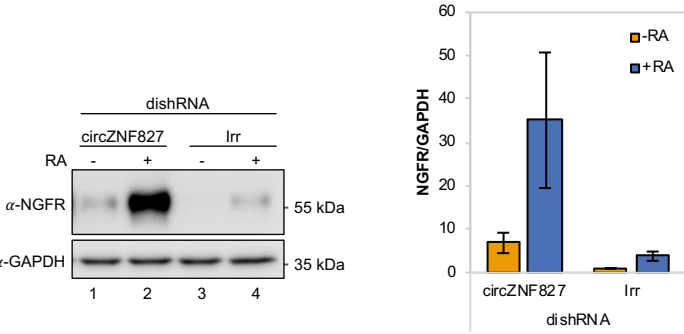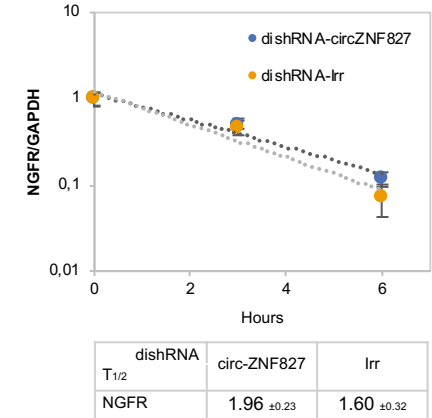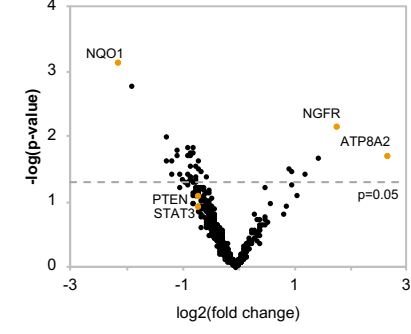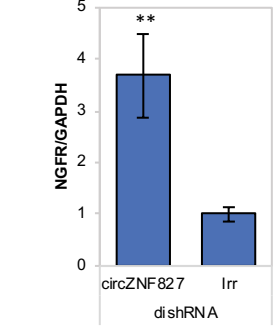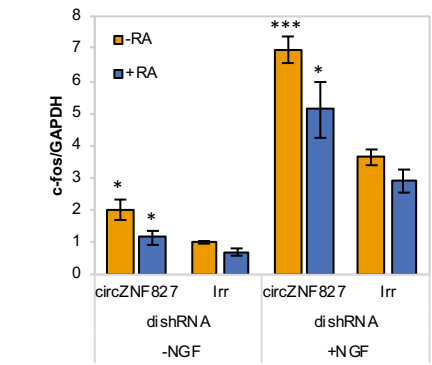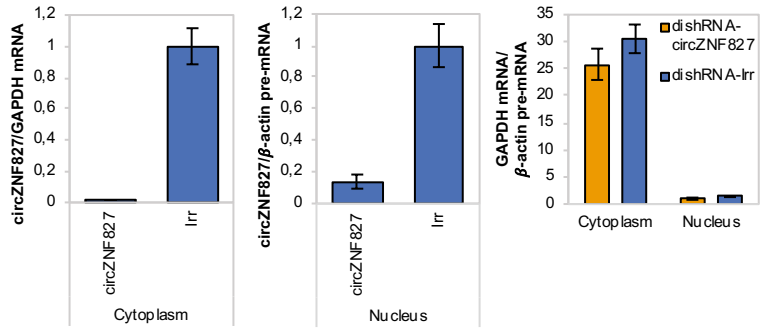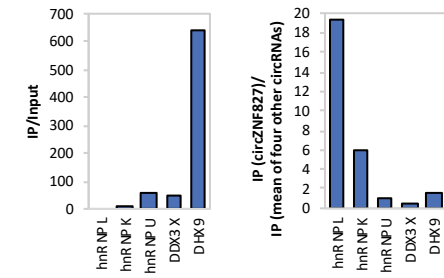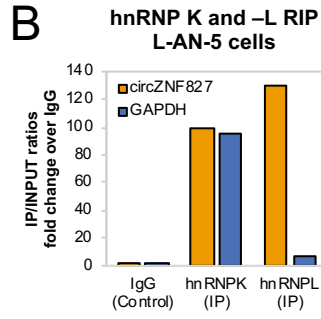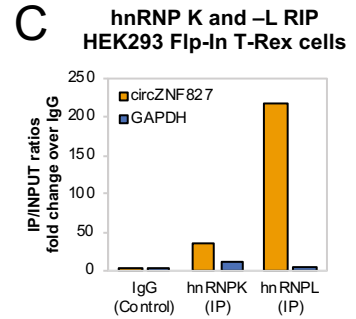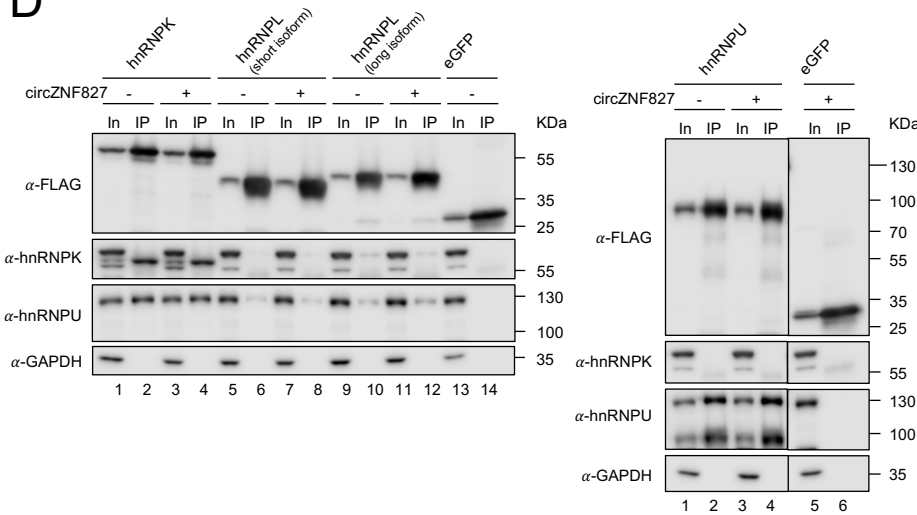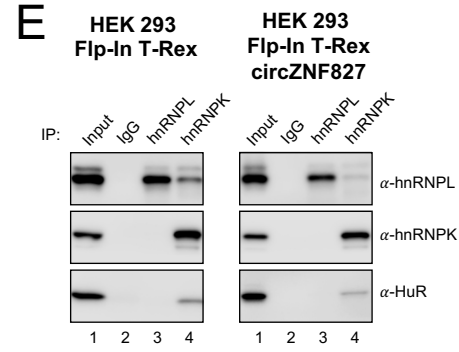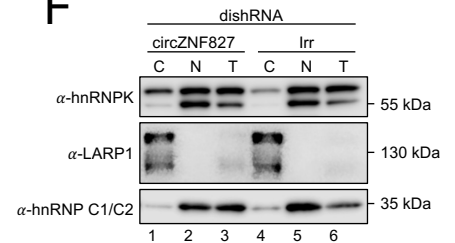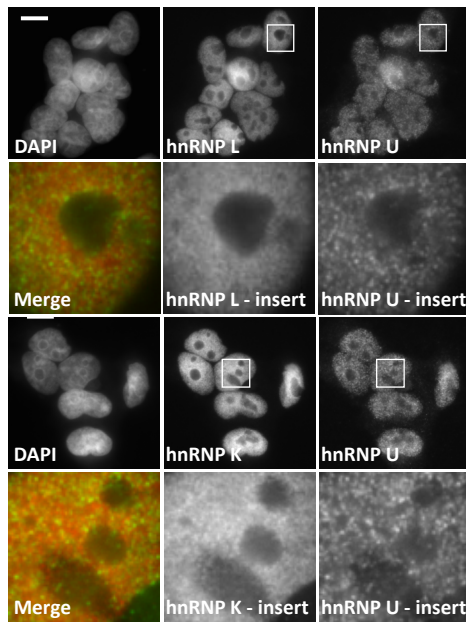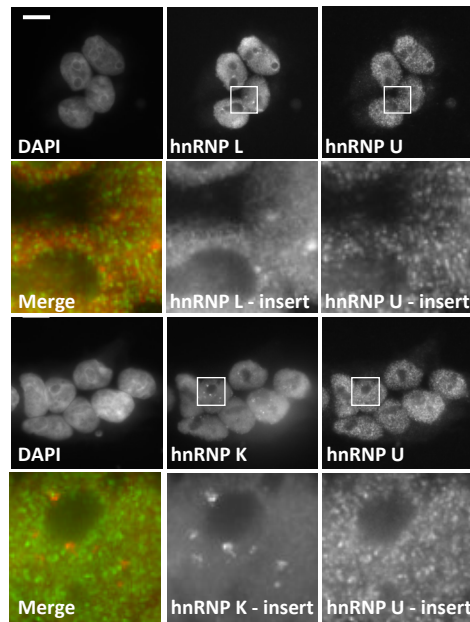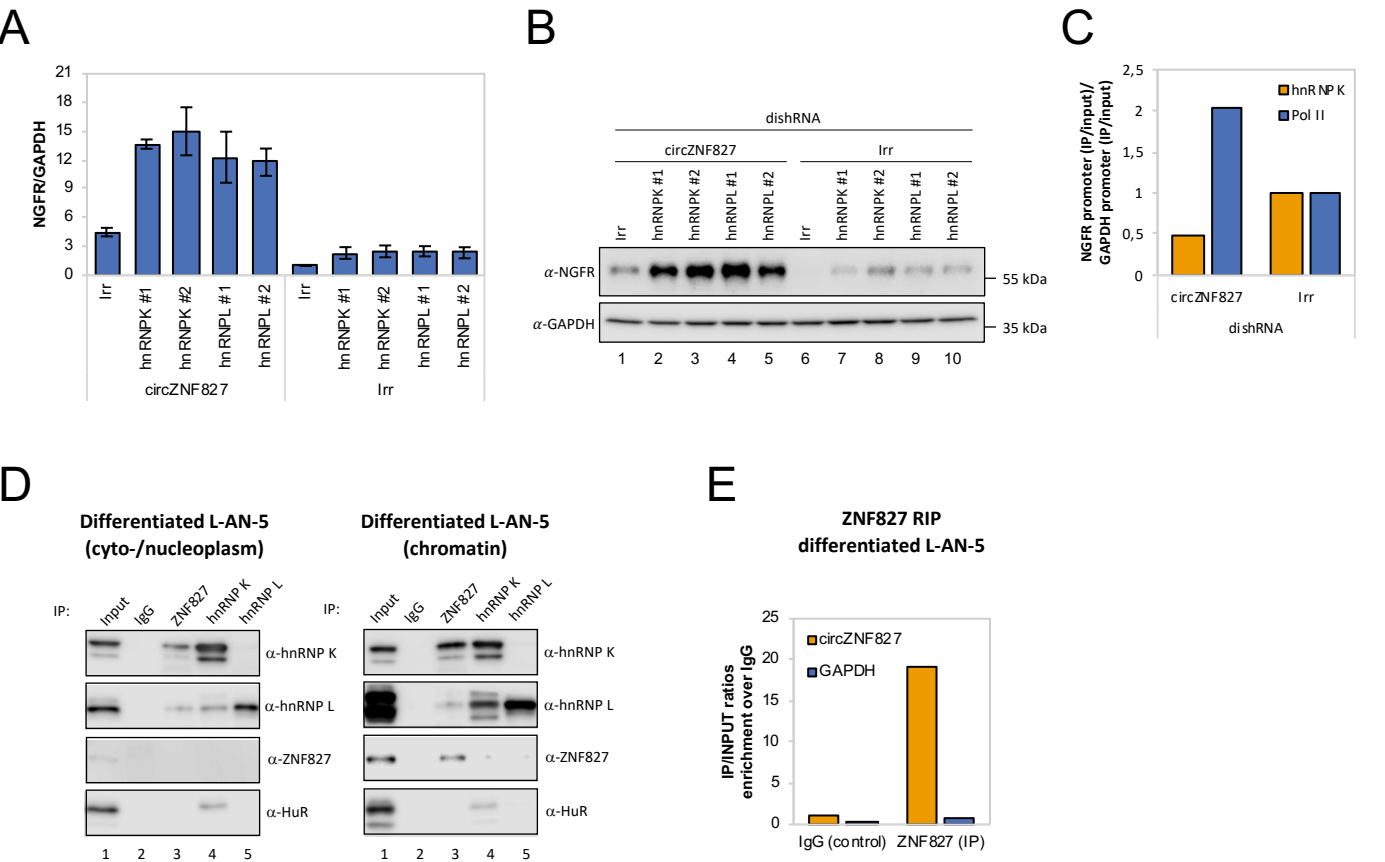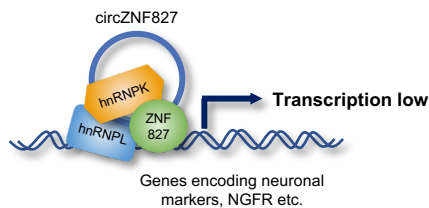
Figure 7

Normal circZNF827 level

circZNF827

hnRNPK

hnRNPL

ZNF 827

Transcription low

Genes encoding neuronal
markers, NGFR etc.

Low circZNF827 level

hnRNPK

ZNF 827

hnRNPL

Transcription high

Genes encoding neuronal
markers, NGFR etc.